Rapport De Projet

4ième Année Département Signaux et Télécommunications

Design Of Integrated And Fiber Optical Micro-Ring Resonators For Telecommunications

Clément Becquet
Author, ESIEE Engineering Paris

Maxime Sother
Author, ESIEE Engineering Paris

Dr. Paul Urquhart
Supervisor, Universidad Pública de Navarra

Pamplona, August 2010

Universidad Pública de Navarra
Public University of Navarra

Escuela Técnica Superior de Ingenieros Industriales y de Telecommunicación

ESIEE Engineering Paris

Ecole Supérieure d'Ingénieurs en Electronique et Electrotechnique

Abstract

This project is a theoretical study of multiple coupled ring resonators, which can be used as demultiplexing filters in optical transmission systems, especially DWDM. We have chosen two approaches: analytical and numerical. Our aim is to design a box-like filter, which is the best spectral profile for most of the modulation formats existing. Therefore, we compare different multiple coupled ring structures and we use different techniques to design them.

We use the compound ring resonator theory formulated by Elshoff and Rautenberg [1] and that formulated by P. Urquhart to calculate analytically the transfer functions of one-, two-, three-, and four-ring resonators. We perform a numerical method to calculate transfer functions of N-ring resonators. The two methods (analytical and numerical) are compared to ensure that the numerical approach is valid for the rest of our calculations.

With the analytical method we make a study of the Vernier effect, with three- and four-ring resonators. The rings have different circumferences but they are in the ratio of two integers, as in Vernier rulers, and we study different kinds of symmetry between these circumferences. With the numerical method we calculate the transfer function of N-ring resonators with different symmetry categories between the coupling ratios.

We investigate the influence of waveguide losses and the fabrication errors in the effective reflectances. Finally, we present an application of the ring resonators to a DWDM signal modulated with a bipolar non-return-to-zero code, to indicate how it can be used in a system.

Acknowledgement

We would like to thank our project supervisor Paul Urquhart for all the support he brought to us during these four months. The lectures, advice, ideas and corrections he gave us were always very helpful.

We would also like to thank Marcel Elshoff and Oscar Rautenberg for the very good work they did on "Design and Modelling of Ring Resonators Used as Optical Filters For communications Applications". It helped us a lot to understand the subject of our project.

We wish to thank Jean-Luc Polleux for connecting us with Paul Urquhart and suggesting the Universidad Pública de Navarra (UPNA).

Table Of Contents

Authorship

1 Introduction……Sother

2 Theory Of Ring Resonators……Becquet and Sother

3 Analytical And Numerical
Methods: Comparison……Becquet and Sother

4 The Vernier Effect: Three- And Four-Ring Resonators……Becquet

5 N-ring Resonators……Sother

6 Waveguide Losses And
Effective Reflectance Errors……Becquet and Sother

7 Application Of A Bipolar Non-Return-To-Zero Code……Sother

8 Conclusion……Becquet

1 Introduction

With the worldwide rapid growth in the exchange of data (internet, digital television, etc) the main transmission means for high capacities, which are optical communications, are going to be increasingly present. Indeed, optical fibre is now being installed in the home (FTTH). This will increase the required bandwidth everywhere, including the core networks. Therefore, we must increase the capacities of each fibre.

Most of the optical transmission systems use some form of wavelength division multiplexing (WDM). There are two categories of wavelength division multiplexing: Coarse (CWDM) and Dense (DWDM). CWDM is the cheaper option but the channel spacing is 20 nm and we are limited to 18 channels [2]. DWDM is the most widely used technique in regional, national and international telecommunication, mostly because today's DWDM systems use 100 GHz or even 50 GHz channel spacing for up to 160 channel operation [3]. In a context of increasing of the capacities of each fibre we must use more DWDM with more channels per fibre and greater spectral densities.

The number of possible modulation formats for digital transmission on fibres is very large and it is currently an active research domain. It is why we need high performance filters to select individual channels and groups of channels. These filters need to have box-like spectral profiles, low excess losses and good depths of modulation. Until now we have used thin film filters, which are reliable and low cost but they might not be appropriate for very high density WDM. Therefore, we have a continuing need for improved filter performance. Moreover, in future, in response to new modulation formats, we might need some very special spectral profiles from our optical filters. Therefore, we need to study all the possibilities of improvement in optical filters; compound ring resonators are certainly one of these possibilities.

Elshoff and Rautenberg designed one-, two-, and three-ring resonators with the same circumferences [1]. We have used their equations to develop analytically three- and four-ring resonator transfer functions with different circumferences. We also used their work on N-ring resonators to develop numerically the transfer functions with N rings. All of these results are presented in this report.

In Chapter 2 we explain the theory of ring resonators and the matrix formulation. Then in Chapter 3 we perform a comparison between the analytical method and the numerical method to enssure that both techniques are valid. Therefore, in Chapter 4 we are able to use the numerical approach to design three- and four-ring resonators, in which the rings have different circumference but these circumferences are determined by the Vernier effect. In Chapter 5 we apply our numerical method to design N-ring resonators with different symmetry categories. In Chapter 6 we examine the influence of losses and errors in the effective reflectances. Finally, in Chapter 7 we present an example of a filter which can be used in DWDM with a bipolar NRZ modulation.

2 Theory Of Ring Resonators

2.1 Introduction

The objective of this chapter is to explain the theory used in our project and so enable the reader to understand the explanations in the subsequent chapters. It starts with a presentation of Wavelength Division Multiplexing (WDM), a very common technique used in optical transmission. Thereafter, ring resonators and optical resonators in general are described, their equations are explained and, as an illustration, some transfer functions are plotted. We also define the concept of free spectral range and show how it is related to ring circumference. The matrix theory of ring resonators is also briefly treated in this chapter.

2.2 Wavelength Division Multiplexing

To understand the theoretical context of this project, it is required to know about Wavelength Division Multiplexing (WDM), which is a technique used in optical fibres. The aim of WDM is to transmit many channels of different wavelengths on only one optical fibre. In this way we can augment the capacity at an acceptable cost. The principle is to multiplex the different wavelength signals at the input of the optical fibre and to demultiplex them at its output before they enter the optical receivers. There are two categories of WDM: “Coarse” WDM and “Dense” WDM. CWDM operates with a wavelength spacing of nominally 20 nm between each channel [2]. The objective is to enable the use of low-cost components, especially uncooled lasers. In contrast, DWDM requires very narrow line spacing (from 0.8 nm to only 0.1 nm, which corresponds to 100 GHz down to 12.5 GHz in terms of frequency)[3]. As illustrated in Figure 2.1, the International Telecommunications Union (ITU) has standardised six different wavelength bands from 1260 nm to 1675 nm [4].

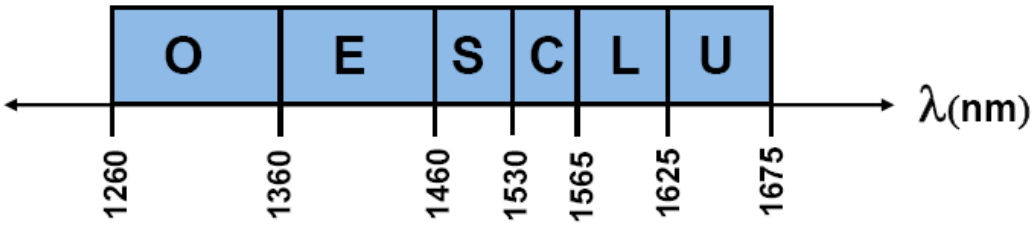

Fig 2.1 *Representation of the International Telecommunications Union standardised wavelength bands for optical transmission. The names of the bands are from the smallest to the largest wavelength: "original", "extended", "short", "conventional", "long" and "ultra-long"* [4].

Due to the fact that it is where the fibre's losses are the lowest, the most commonly used band is the "conventional" band (or C-band), from 1530 nm to 1565 nm. The optical filters presented in this report are band-pass filters used for optical demultiplexing and we anticipate that in many cases they will operate in the C-band to select individual DWDM channels.

2.3 Ring Resonators

This report contains many explanations and simulations involving ring resonators. A ring resonator is a specific type of optical resonator in which light is confined to a single mode waveguide in the form of a circuit, as shown in Figure 2.2.

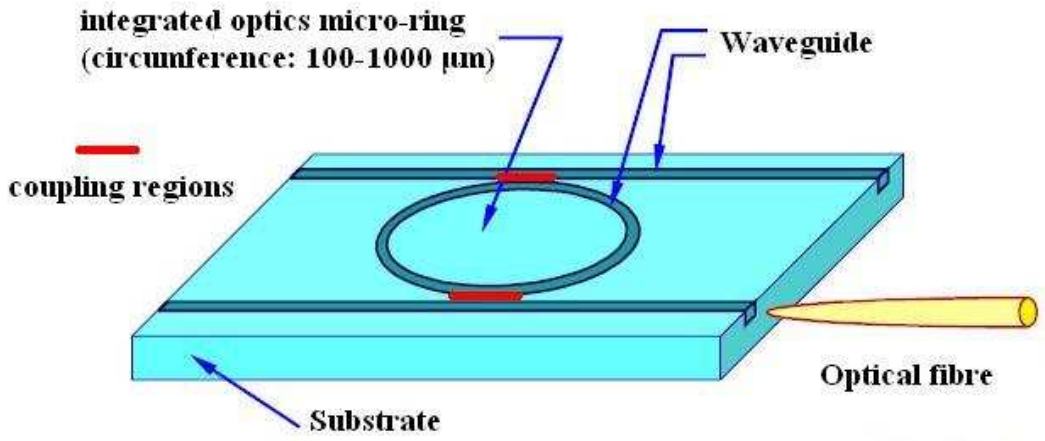

Fig 2.2 *Integrated optical ring resonator showing the inputs, outputs and coupling regions.*

The resonator shown in Figure 2.2 includes two couplers which connect the ring to two waveguides; one is at each side. The couplers are formed by bringing waveguides into close proximity so that their guided fields overlap and there is thus an exchange of energy between them. All waveguides are fabricated in low loss materials and they are most commonly glass. However, for specialist applications, semiconductors or polymers can also be used [5]. Figure 2.2 also shows how some or all of the waveguide ends, at the edge of the chip, are coupled to single-mode optical fibres; the tapered fibre end minimises the losses at the interface. The ring resonators that are of greatest interest in this project are micro-rings, in which the circumference is a few hundred micrometres in order to ensure transfer functions with appropriate spacing between their periodic pass-bands. This aspect is explained further in Section 2.4.

2.4 Optical Resonator Transfer Function

An optical ring resonator is equivalent to a cavity (for example a Fabry-Pérot cavity) created by two parallel mirrors. Each of these mirrors has a transmission coefficient (transmittance) and a reflection coefficient (reflectance). Thus, as shown on Figure 2.3, when a light wave enters the optical resonator, there is some energy that exits from the end of it, and some energy that is reflected. At a specific wavelength that satisfies the resonance condition, energy is stored within the cavity. The resonance condition applies when the cavity length is an integral number of half wavelengths.

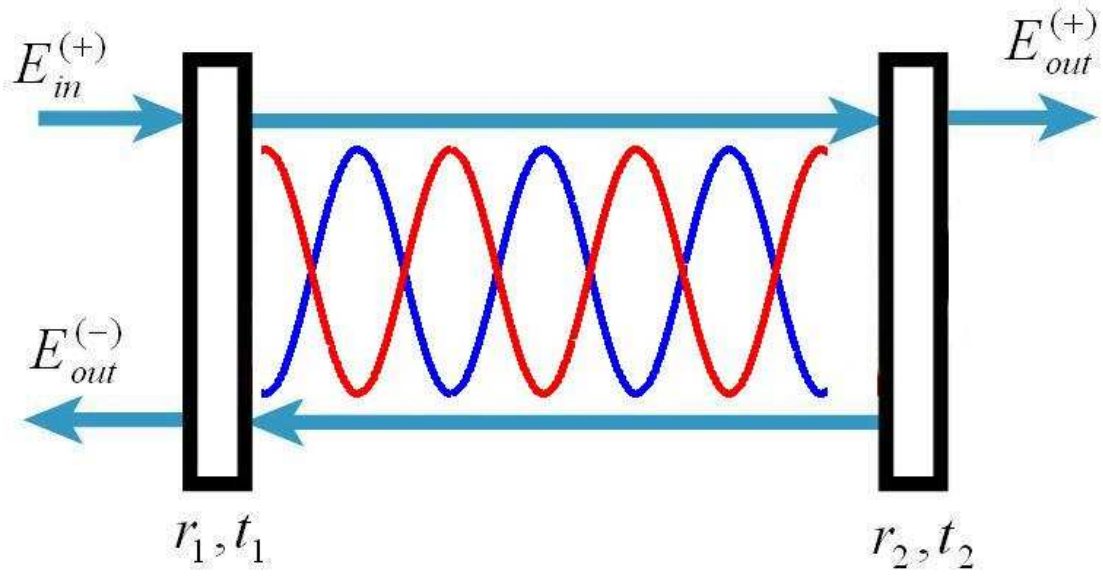

Fig 2.3 *Representation of a light wave entering in an optical resonator. At the resonance, there is a standing wave.*

The equations of the transmitted output of an optical resonator are:

$$\left|\frac{E_{out}^{(+)}}{E_{in}^{(+)}}\right|^2 = \frac{T^2}{(1-R)^2+4\cdot R\sin^2(\beta L)}, \qquad (2.1)$$

Where the constants T and R are given by

$$T = t_1 \cdot t_2 \cdot e^{-\frac{\alpha L}{2}} \qquad (2.2)$$

$$R = r_1 \cdot r_2 \cdot e^{-\alpha L} \qquad (2.3)$$

$\alpha/2$ being the amplitude loss coefficient, β being the propagation constant and L being the length of the cavity. Equations (2.1)-(2.3) were derived by Elshoff and Rautenberg [1].

The effective reflectance, R, determines the shape of the transmission curve of the Fabry-Perot cavity and Figure 2.4 presents some examples of this curve on both linear and logarithmic scales.

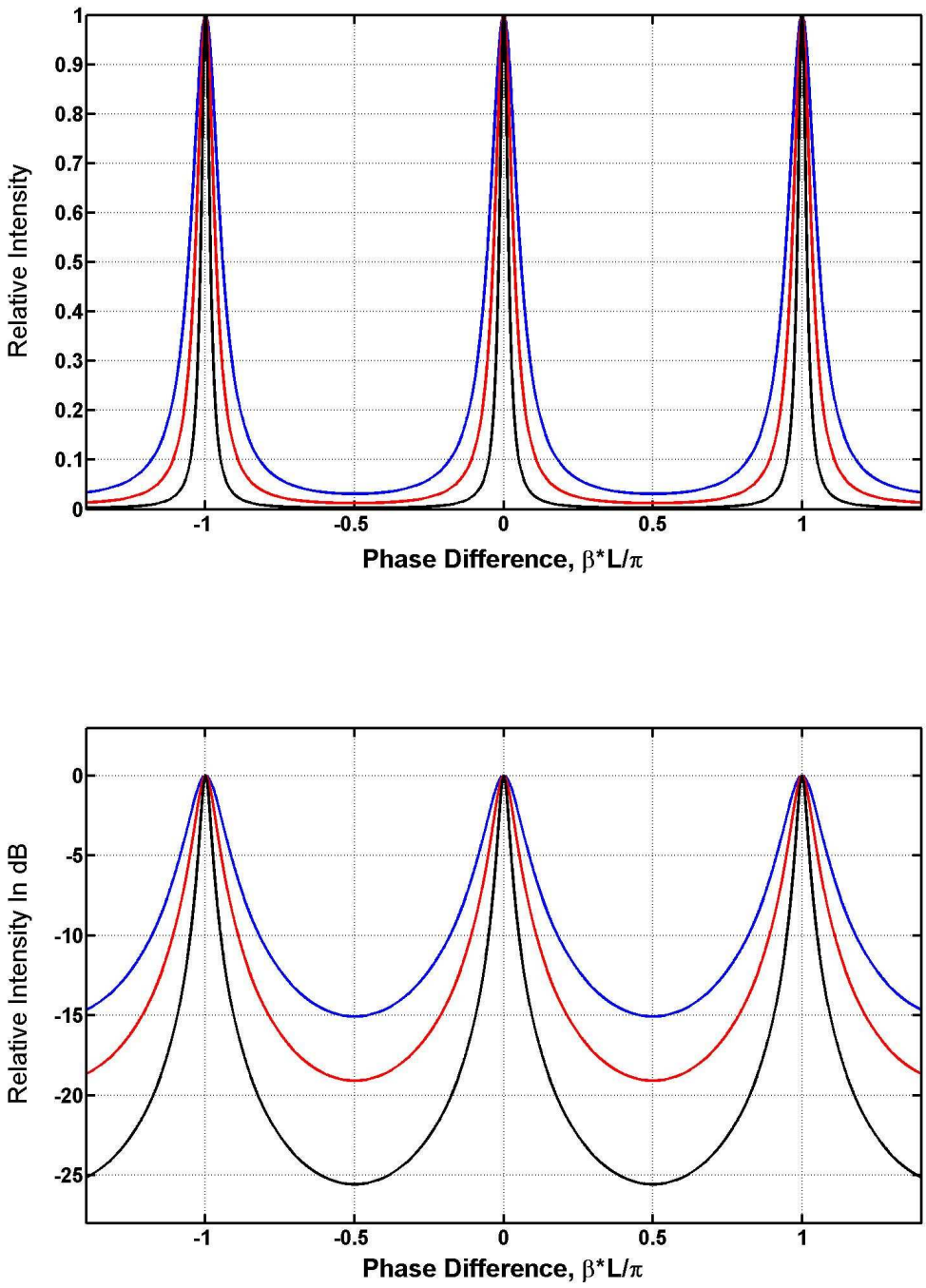

Fig 2.4 *Transfer functions of a Fabry-Perot cavity with different reflectances. From top to bottom on each graph, the reflectances are: R=0.7, R=0.8 and R=0.9.*

The top plot of Figure 2.4 is in linear units and the bottom plot presents the same data on a logarithmic vertical axis. It is clear that the transfer function is periodic with a periodicity of π radians. The peaks occur at 0, ±π, ±2π, … and the minima are at ± π/2, ± 3π/2, ±5π/2, … The space between the peaks is known as the resonator's free spectral range (FSR) and it is derived in Section 2.5. We observe on Figure 2.4 that the depth of modulation increases and the peak narrows with increasing reflectance.

The equations of light intensity of an optical ring resonator are:

$$\left|\frac{E_{out}^{(+)}}{E_{in}^{(+)}}\right|^2 = \frac{T^2}{(1-R)^2+4\cdot R\sin^2(\beta L)}, \quad (2.4)$$

$$T = K_1^{\frac{1}{2}} \cdot K_2^{\frac{1}{2}} \cdot e^{-\alpha L} \quad (2.5)$$

$$R = (1-K_1)^{\frac{1}{2}} \cdot (1-K_2)^{\frac{1}{2}} \cdot e^{-\alpha L} \quad (2.6)$$

K_1 and K_2 being the coupling coefficient of the two couplers of Figure 2.2. L is the distance between the two coupling regions. It can be seen that Equations (2.1) and (2.4) are identical and this is why we can identify R and T, given by Equations (2.5) and (2.6), respectively, as the ring's effective reflectance and effective transmittance. Consequently, Figure 2.4 applies equally to Fabry-Pérot cavities and ring resonators.

It is possible to realise compound resonators composed of several micro-rings placed in all kinds of configurations. Moreover, it is also possible to use micro-ring resonators of different circumferences in these compound structures. In this way, one can change the transfer functions to provide improved filter characteristics. That is one of the most important notions to understand this report, because we present many different resonator designs in the chapters that follow.

2.5 Free Spectral Range of a Ring Resonator

This section describes shows how the free spectral range (FSR) of a ring resonator determines the circumference that must be fabricated.

The resonances occur when $\beta L = 0, \pm\pi, \pm 2\pi, ...$ but $\beta = \frac{2\pi n_{eff}}{\lambda} = \frac{2\pi\nu n_{eff}}{c}$, where ϑ is frequency. Thus the difference in phase between the peaks is π. Therefore, $\Delta\beta L = \pi$ and $\frac{2\,\pi\,\Delta\nu\,n_{eff}\,L}{c} = \pi$. We can now identify the free spectral range, which is given by Equation (2.7).

$$\Delta\nu = F.S.R = \frac{c}{2n_{eff}L} \qquad (2.7)$$

n_{eff} is the effective refractive index of the waveguide and L is the ring circumference. Δν is frequency in Hertz.

As an example, we wish the ring resonator to accept every tenth channel and to reject the others. We assume that we are operating on the 100 GHz grid. We therefore need use to calculate the corresponding ring circumference L. $\Delta\upsilon = 10*100GHz = 10^{12}\,Hz$, $c = 3*10^{8}\,m/s$ and $n_{eff} = 1.5$ (it is a typical value for glass).

Thus $L = \frac{c}{2n_{eff}\cdot\Delta\upsilon} = \frac{3*10^{8}}{2*1.5*10^{12}} = 10^{-4}\,metres$ = 100 µm

Clearly, the ring needed is very small. This is important for two reasons: it imposes constraints on the fabrication technology and small radius rings are subject to bending losses. We consider the issue of losses in Chapter 6. Moreover, our use of the Vernier effect in Chapter 4 is justified partly on the basis that it is a means to avoid using small radius rings.

2.6 Matrix Formulation

A good way to analyse an optical filter is to observe its relative intensity transfer function, which is the square of the modulus of the complex field transfer function. For each coupler we have four equations. The equations of the first coupler are written from (2.8) to (2.11); these equations have been derived by Elshoff and Rautenberg [1].

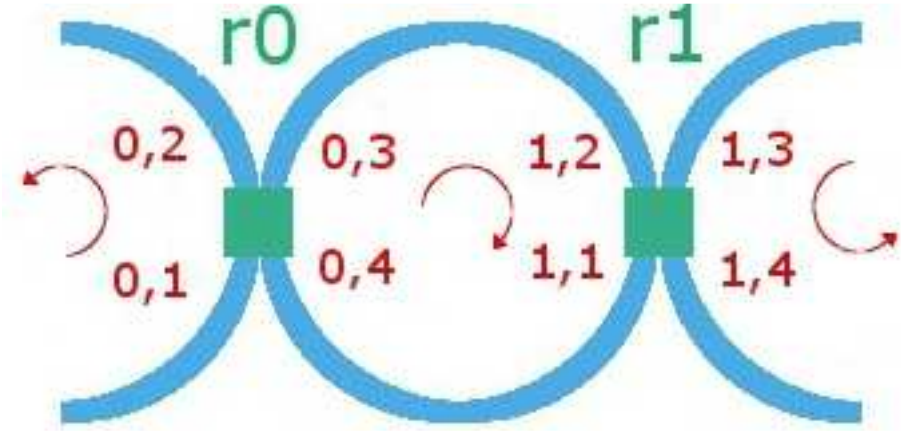

Fig 2.5 *One ring resonator, the arrows representing the direction of the light, in green is the couplers with their coupling ratios.*

When light is launched only via "point 0,1", marked on Figure 2.5, the waves circulate clockwise within the ring, as shown by the arrows. In these conditions we can write the four equations relevant to the first coupler r_0:

$$E_{0,1} = \text{input} \tag{2.8}$$

$$E_{0,2} = r_0 \cdot E_{0,1} + t_0 \cdot E_{0,4} \tag{2.9}$$

$$E_{0,3} = r_0 \cdot E_{0,4} + t_0 \cdot E_{0,1} \tag{2.10}$$

$$E_{0,4} = E_{1,1} \cdot e^{\delta_{1/2}} \tag{2.11}$$

With

$$\delta_{1/2} = \left(\frac{-\alpha}{2} + i \cdot \beta\right) \cdot \frac{L}{2} \tag{2.12}$$

To formulate a complete structure for a single ring resonator, we need the four equations of the second coupler from (2.13) to (2.16), which have also been derived by Elshoff and Rautenberg [1].

$$E_{1,1} = r_1 \cdot E_{1,2} + t_1 \cdot E_{1,3} \quad (2.13)$$

$$E_{1,2} = E_{0,3} \cdot e^{\delta_{1/2}} \quad (2.14)$$

$$E_{1,3} = E_{1,3} \quad (2.15)$$

$$E_{1,4} = r_1 \cdot E_{1,3} + t_1 \cdot E_{1,2} \quad (2.16)$$

If we substitute Equations (2.8)-(2.11) into Equations (2.13)-(2.16) we obtain two equations which have this form:

$$E_{0,2} = a_{11} \cdot E_{0,1} + a_{12} \cdot E_{1,3} \quad (2.17)$$

$$E_{1,4} = a_{21} \cdot E_{0,1} + a_{22} \cdot E_{1,3} \quad (2.18)$$

Equations (2.17) and (2.18) can also be written as a matrix presented Equation (2.19). This matrix represents a single resonator.

$$\begin{bmatrix} E_{0,2} \\ E_{1,4} \end{bmatrix} = \begin{bmatrix} a_{11} & a_{12} \\ a_{21} & a_{22} \end{bmatrix} \cdot \begin{bmatrix} E_{0,1} \\ E_{1,3} \end{bmatrix} \quad (2.19)$$

The greatest advantage of matrix formulation is that we can easily multiply many matrices, so we can extend the formulation of a single ring resonator to a multiple ring resonator. The formulation that leads to Equation (2.19) is the basis for the theory in the following chapters.

3 Analytical And Numerical Method: Comparison

3.1 Introduction

The transfer function for an N-ring resonator can always be formulated by the appropriate use of complex electric fields. In principle it is thus possible to predict the performance of filters of arbitrary complexity through the provision of analytical functions. However, the equations can be very large. The main disadvantages of analytical solutions of the equations are the time that it takes to derive such equations and the fact that it is always possible to make mistakes during calculation. Moreover, as Elshoff and Rautenberg have argued, computer algebra does not necessarily ameliorate the situation. These problems become ever greater as the number of rings is increased and the issue is well illustrated by the size of the transfer function for a four-ring resonator reported in Appendix 1, from which it can be seen that listing the various terms of the intensity equation takes two pages. We therefore need an alternative approach and that is the purpose of the current chapter.

3.2 The Analytical Method

To simulate a four-ring resonator in the analytical way, we used the calculation made by Elshoff and Rautenberg for a three-ring resonator and it was extended to a four-ring resonator by Dr Paul Urquhart. (Readers interested in seeing the full calculation should ask its author at paul.urquhart@unavarra.es).

The final equations developed by Urquhart are very long. It is not interesting to present it in this report. Nevertheless, the complete formula is available in Appendix 1 of this report.

3.3 The Numerical Method

We have created a Matlab function to calculate and plot the transfer functions of different ring resonators with the same circumference. To make this Matlab function the first thing to do is to define the phase change because it is the horizontal coordinate of the graphs that we plot. The phase is stated as $\frac{\beta * L}{\pi}$, where β is the propagation constant of the waveguide, given by $\frac{2\pi n_{eff}}{\lambda}$, in which n_{eff} is the effective refractive index. L is the waveguide's length. The product βL is in radians and we normally plot our graphs over the range $-3 \leq \frac{\beta * L}{\pi} \leq +3$. During this interval we can show several of the peaks on the periodic transfer function. The product βL is directly proportional to the absolute frequency of the light (both vary as the inverse of the wavelength).

We have written a vector function in Matlab, which contains all the possible values of β depending on the number of points we want to use when plotting the transfer functions (this is the parameter M). We now can use our vector to build another vector, which contains all the values of the parameter given in Equation (3.1).

$$\delta = \left(\frac{-\alpha}{2} + \mathrm{i} \cdot \beta\right) \cdot \mathrm{L} \qquad (3.1)$$

The term δ is the argument of the exponential terms within the formulation of the transfer functions and it contains the waveguide loss coefficient α (meters^{-1}). The Matlab function that we have written is stated in Figure 3.1.

```
%For Loop to make the calculation of the M+1 possibilities of beta
  for p = 0:1:M
  beta(1,p+1) = (-3*pi + p*pi/(M/6))/L ;
  delta(1,p+1) = (-alpha/2 + 1i*beta(1,p+1))*L ;
```

Fig 3.1 *Part of the Matlab function which creates the two vectors β and δ.*

As explained Chapter 2, ring resonators can be formulated using matrices; these matrices depend on δ and we have one 2 x 2 matrix for each δ. We create a 2M x 2M matrix, which regroups all of the 2x2 matrices, as can be seen in Figure 3.2.

```
A(1+2*p,1+2*p) = (-r0*r1 + (t0^2 - r0^2)*(t1^2 - r1^2) * exp(delta(1,p+1))) / (t0*t1) ;
A(1+2*p,2+2*p) = (r1 + r0*(t1^2 - r1^2) * exp(delta(2,p+1))) / (t0*t1);
A(2+2*p,1+2*p) = (-r0 * exp(-delta(1,p+1)) - r1 * (t0^2 - r0^2)) / (t0*t1) ;
A(2+2*p,2+2*p) = (exp(-delta(1,p+1)) - r0*r1) / (t0*t1) ;
```

Fig 3.2 *Part of the Matlab function which creates a 2M x 2M matrix.*

One of the advantages of using the numerical method is the fact that Matlab can easily perform matrix calculation. We can thus multiply the matrices or raise them to a power as shown in Figure 3.3.

```
AN(1+2*p:1:2+2*p,1+2*p:1:2+2*p) = A(1+2*p:1:2+2*p,1+2*p:1:2+2*p)^(N/2);
```

Fig 3.3 *Example of Matlab matrix calculation. The matrix A is divided into 2x2 matrices. All such matrices are raised to the power of N/2 and then incorporated into the 2M x 2M matrix.*

The next step is to extract the amplitude transfer function which is shown in Equation (3.2). To do that we have to create a vector E, which contains all possible values of the amplitude transfer function. Each value of E corresponds to a 2x2 matrix contained in the 2M x 2M matrix, Q. Figure 3.4 shows how we can do that with Matlab.

$$\frac{E_{out}}{E_{in}} = \frac{q_{22} \cdot q_{11} - q_{12} \cdot q_{21}}{q_{22}} \qquad (3.2)$$

```
E(1,p+1) = ( Q(2+2*p,2+2*p) * Q(1+2*p,1+2*p) - Q(1+2*p,2+2*p) * Q(2+2*p,1+2*p) ) /( Q(2+2*p,2+2*p) );
```

Fig 3.4 *Calculation of the amplitude transfer function represented by the vector E, which is calculated from the 2M x 2M matrix Q.*

To calculate the relative intensity transfer function we square the modulus the vector E, as shown in Figure 3.5.

```
I(1,p+1)= abs(E(1,p+1))^2;
end
```

Fig 3.5 *Calculation of the relative intensity transfer function represented by the vector I. The operator "end" means that the 'for loop' which begun at the start of the Matlab function is finished.*

Finally, we calculated the same transfer function in two different ways: one is by the analytical method and another is with the numerical method to ensure that the two techniques give us the same results. We did this for a four-ring resonator with identical circumferences and the results are plotted in Figure 3.6. The two methods are in very good agreement because of the close proximity of the curves. This gives us the confidence to use our numerical method to explore the transfer functions of resonators with much larger numbers of rings in the chapters that follow.

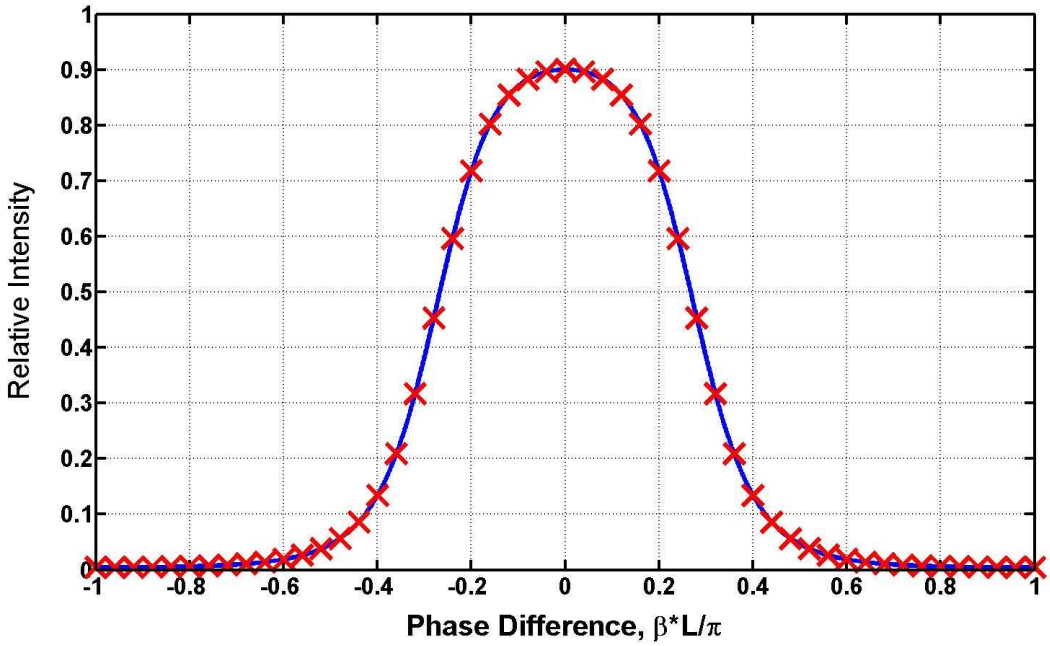

Fig 3.6 *Two transfer functions in linear units for a four ring resonator with identical circumferences. The effective reflectances are r_0 = 0.2, r_1 = 0.65, r_2 = 0.9, r_3 = 0.65, r_4 = 0.2. The red crosses represent the transfer function calculated by the numerical method and the blue line represents the transfer function calculated by the analytical method.*

In conclusion, in this chapter we have argued that, although analytical solutions can provide transfer functions of resonators of arbitrary complexity, the expressions are very large and subject to mistake. We have therefore developed an alternative numerical method which provides solutions that are agreement with the analytical approach.

4 The Vernier Effect: Three- And Four-Ring Resonators

4.1 Introduction

The aim of this chapter is to present the Vernier Effect: its basic principle, how it can be used and in which domains it is applied, especially to micro-ring resonators. It shows how this particular effect could be very useful in designing filters based on optical ring resonators. We concentrate on three- and four-ring structures.

The micro-ring resonators study begins with four-ring designs, using rings with different circumferences. Several kinds of symmetries are tested in this part in order to find the best possible configuration. Then a particular configuration of ring resonator with three different circumferences is presented.

4.2 The Vernier Effect

The Vernier ruler is best known from traditional applications in mechanical engineering in order to measure distances accurately using simple means. The effect is illustrated by the Vernier Scale, which is an additional moving scale placed on a regular scale, and it allows more precise distance measurements to be made (the precision is approximately of 0.01 mm). The second scale has nine equally spaced graduations per centimetre instead of ten. The zero point of the Vernier Scale is placed at the end of the measured object. If it is between two graduations of the fixed scale, the best aligned pair of graduation of the fixed and Vernier scale will determine the most precise digit. An illustration of a Vernier ruler and its implementation is presented in Figure 4.1.

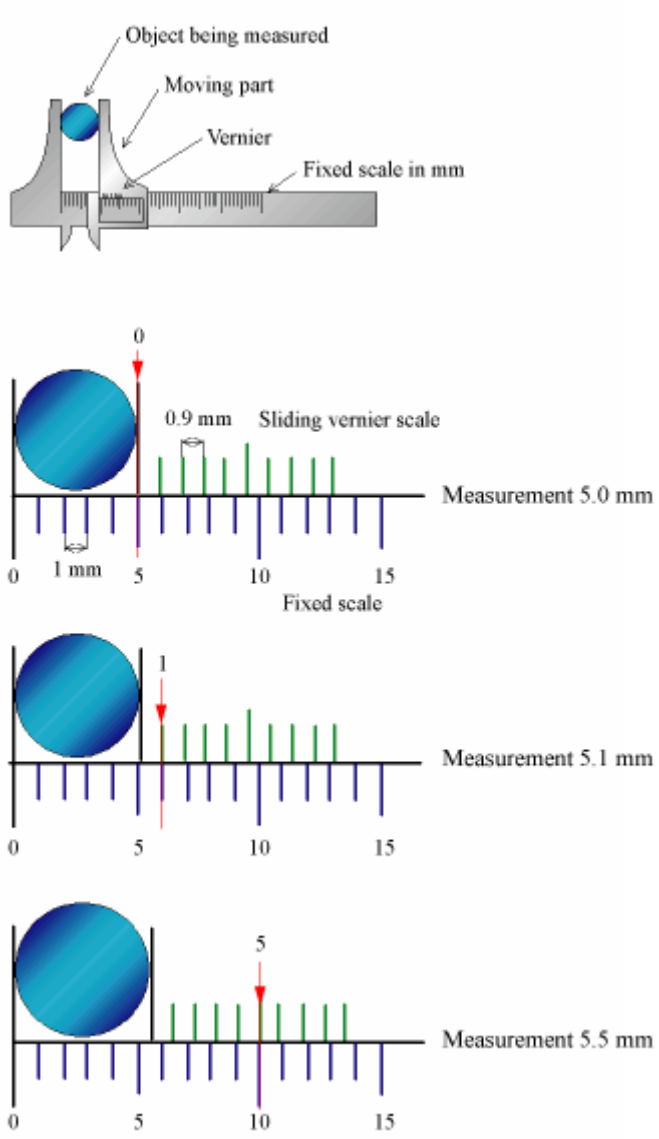

Fig 4.1 *Illustration of the Vernier principle* [6].

The Vernier effect is used in optics, especially with lasers. In this case it is called the optical Vernier effect, but it is also used in many different domains, such as mechanics, electromagnetism and acoustics. In our case, the Vernier effect is created by designing a ring resonator with different circumference rings. The circumferences are ideally in the ratios of two integers, such as 9:10 or 7:8, which do not have a common factor. The transfer functions of two rings of different circumferences have different periods. A "super resonance" effect is created when the peaks of the transfer function of each ring coincide, as shown in Figure 4.2.

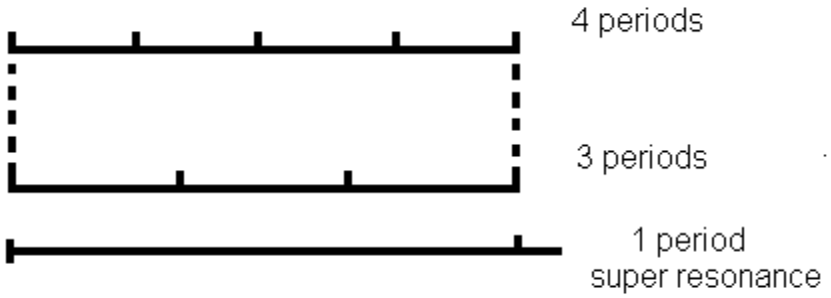

Fig 4.2 *Illustration of the Vernier effect with the super resonances. In this example the ratio of the intervals is 3:4 but other ratios can be used, provided that they are integers.*

4.3 Study of four-ring resonators

In this study, all kinds of possible symmetries involving two pairs of rings with the same circumferences are considered. There are six possibilities, as illustrated in Figure 4.3.

A 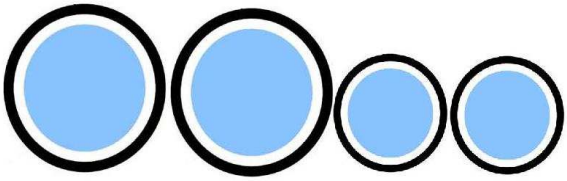

B 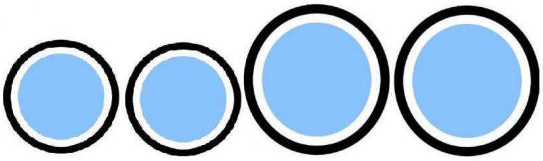

C 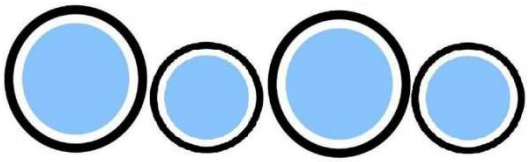

D 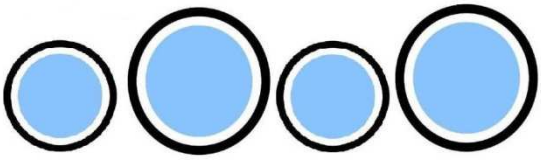

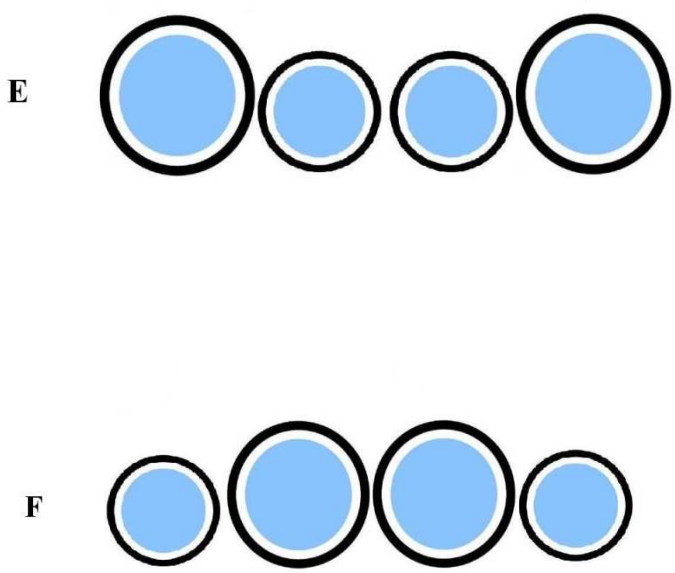

Fig 4.3 *The six different resonator configurations possible with four rings of two different circumferences. The categorization A,…,F is referred throughout this chapter.*

During the simulations, it became clear that some of the combinations, shown in Figure 4.3, do not present useful results all the time. It depends on the parameters involved (such as the ratio of the circumferences and the effective reflectances). This report therefore presents only the potentially applicable results in each case.

Figure 4.4 plots detail from two transfer functions, both of which are for four-ring resonators. The curves concentrate on the most prominent peak. Curve a is when all four rings are of equal circumference and Curve b is when there are two ring circumferences, being in the ratio of 3:4. In Curve b the rings were in Configuration A, shown in Figure 4.3.

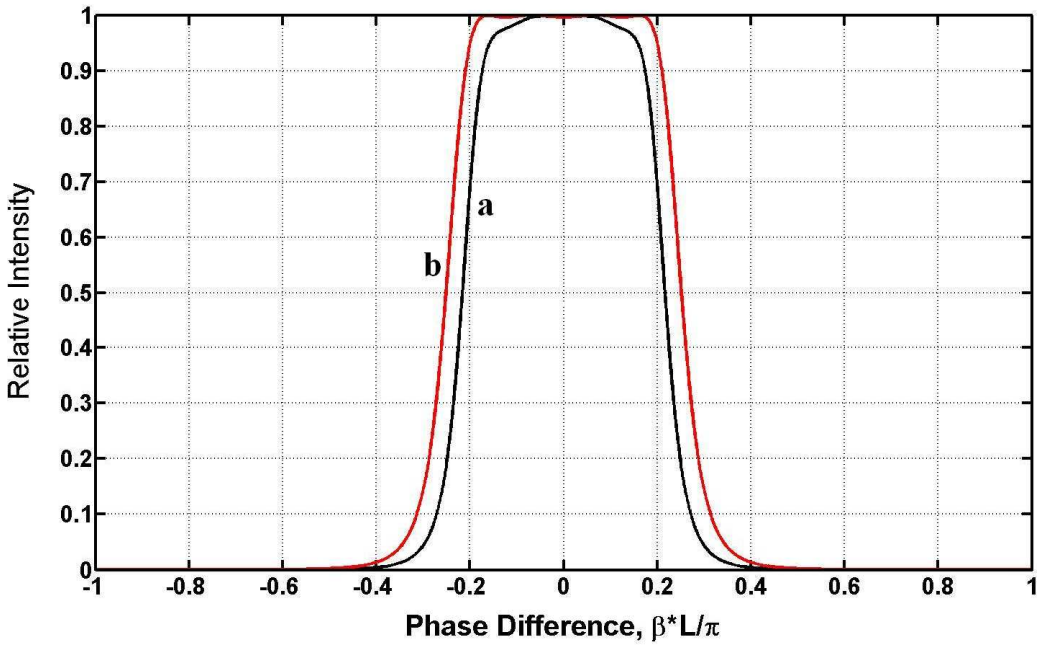

Fig 4.4 Comparison of the peaks of the transfer functions of a four-ring resonator. Curve a: equal ring circumferences and Curve b: two different circumferences (ratio 3:4) that conform to Configuration A in Figure 4.3.

As we can see on Figure 4.4, the transfer function's peak of Curve b is larger and more "box-like". That shows that the Vernier effect could be very useful in this kind of filter design in which the "box-like" shape is needed.

We now study the transfer functions of compound resonators with different ring sizes in greater depth. Our first approach is to use rings with very close circumferences because we can thus avoid the need to fabricate waveguides with small bend radii and their associated losses. Figure 4.5 is the results of a simulation where the circumferences are in the proportions of 9:10.

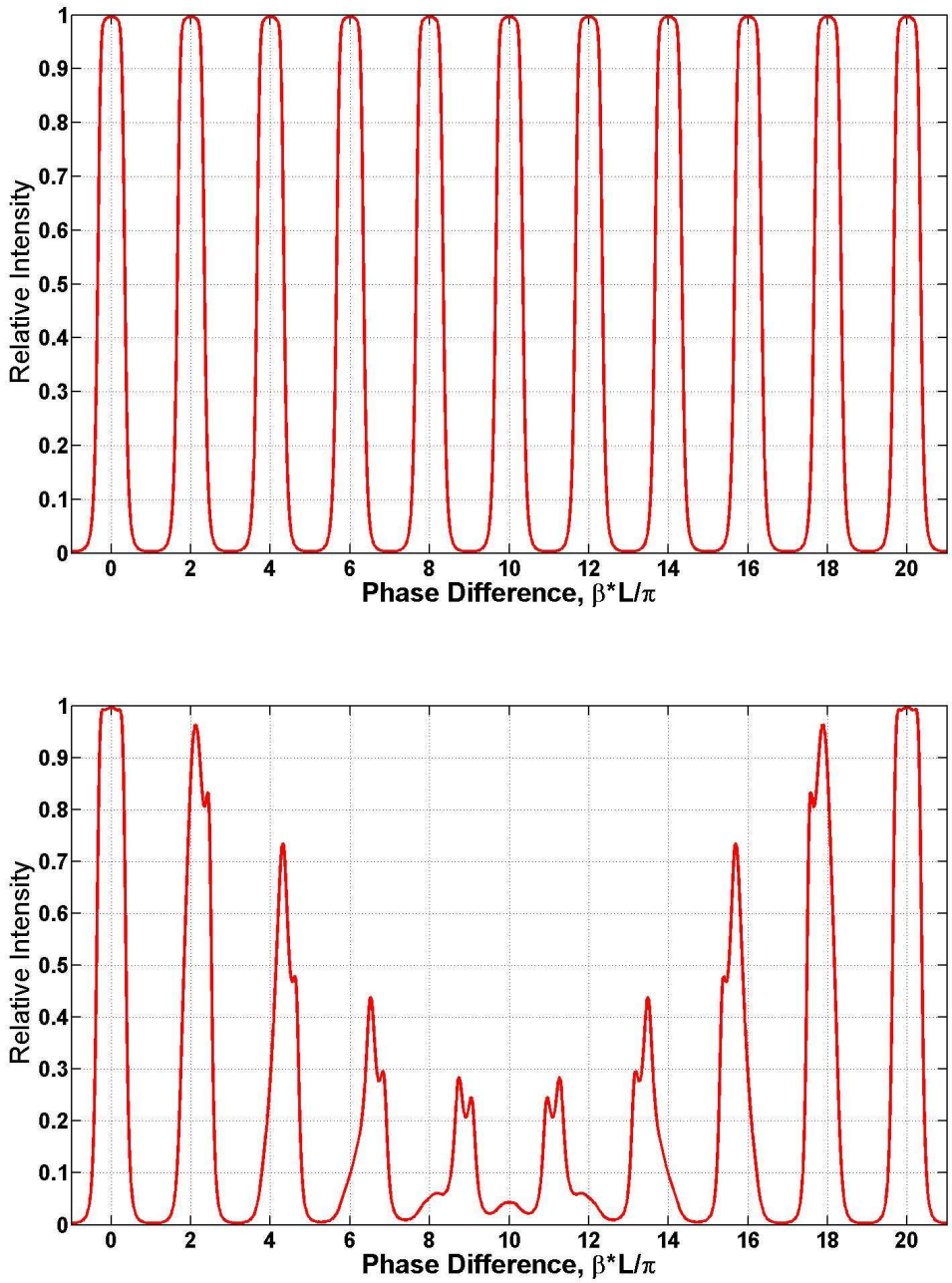

Fig 4.5 *Transfer function of a four ring resonator with* $r_0 = 0.5$, $r_1 = 0.8$, $r_2 = 0.8$, $r_3 = 0.6$, $r_4 = 0.2$. *Top: equal ring circumferences. Bottom: Ring circumferences of 9:10 with the pattern shown in B of Fig 4.3. The vertical axis is linear.*

Figure 4.5 (bottom plot) shows that the subsidiary (or auxiliary) peaks are very high. It is absolutely necessary to reduce them to avoid cross-talk when they coincide with adjacent channels. A Matlab program based on a systematic method to remove these peaks was used and the results are displayed in Figure 4.6.

A

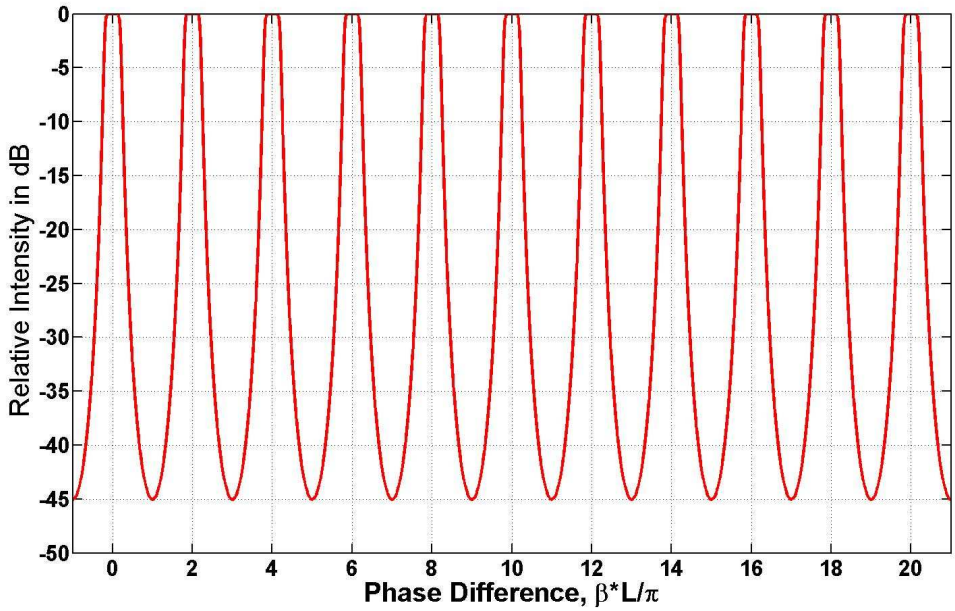

B

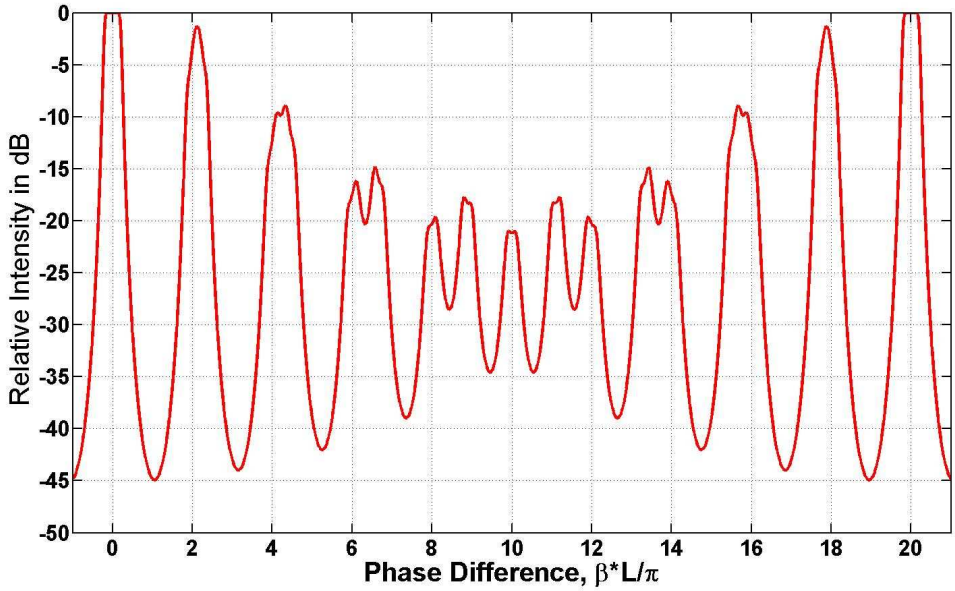

Figure continued on next page.

C

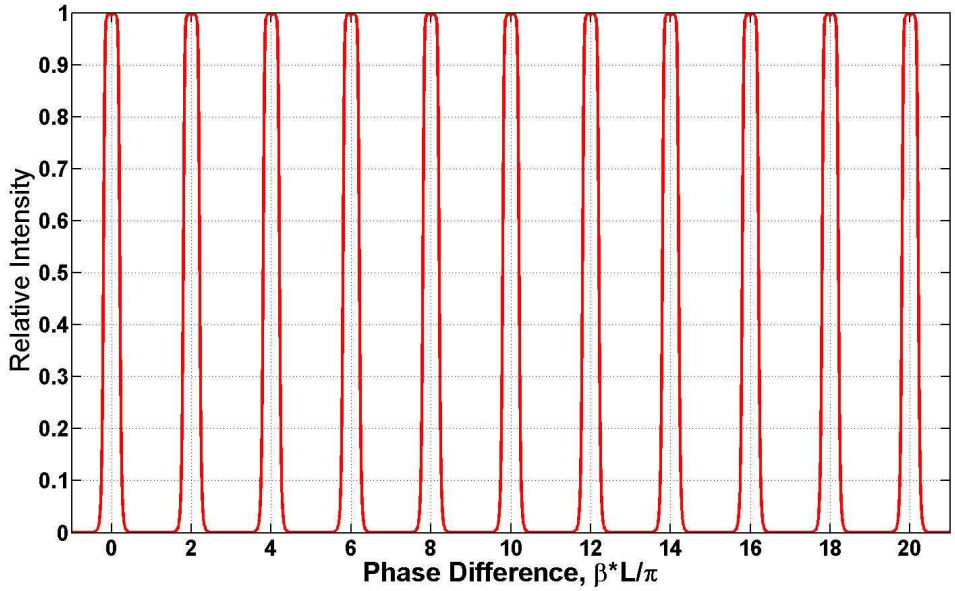

D

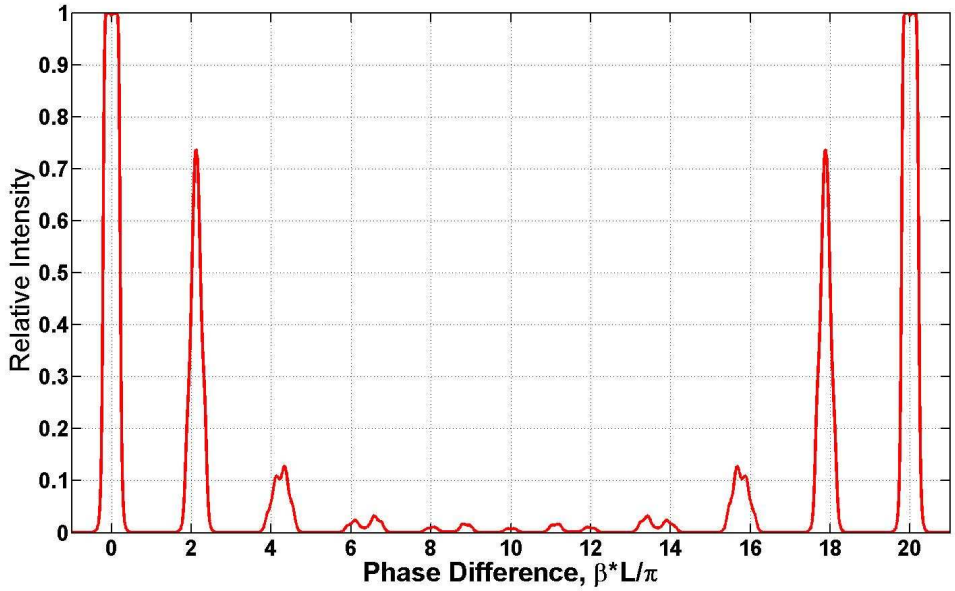

Fig 4.6 *Transfer function of a four ring resonator with* $r_0 = 0.58$, $r_1 = 0.91$, $r_2 = 0.94$, $r = 0.88$ *and* $r_4 = 0.52$. *Curves A and C are with equal ring circumferences in linear units and in decibels units, respectively. Curve B and D are for rings in the ratio of 9:10 and in the Configuration B of Figure 4.3.*

Figure 4.6 illustrates how the method can be used to attenuate the subsidiary peaks to a certain extent, but they are not small enough to avoid the potential problem of adjacent-channel crosstalk. We can clearly see on Curve B of Fig 4.6 (plotted in dB) that the values are not sufficiently low. That is why the following simulations are orientated towards other configurations of resonators.

It is clear from Figure 4.6 that finding appropriate filtering performance depends of the proportions chosen. By simulating different configurations, we found that 1:3 and 2:3 are good circumference ratios; they can provide a side-band suppression ratio of about 20dB. Some of the transfer functions that we calculated are plotted in Figure 4.7.

A

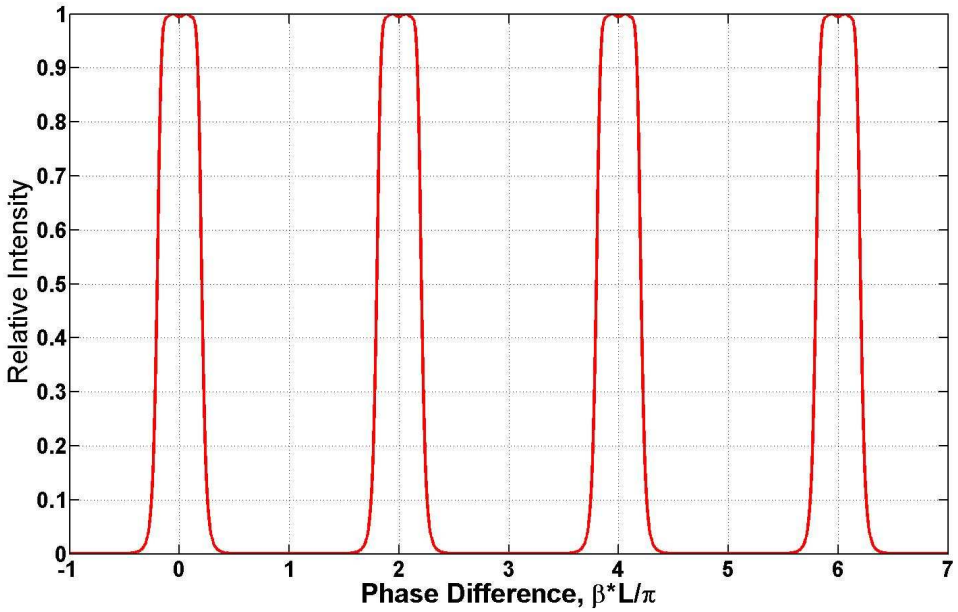

Figure continued on next page

B

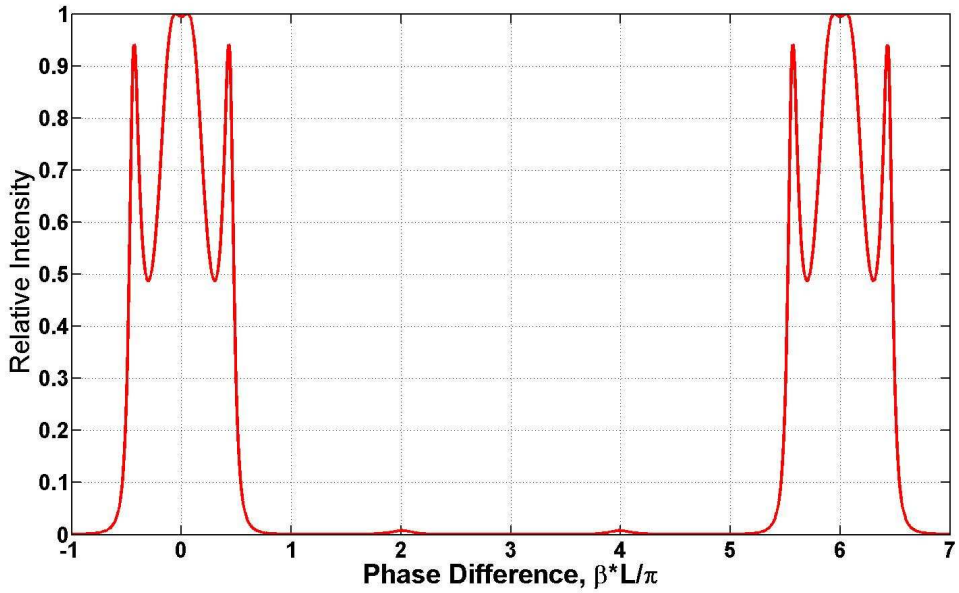

C

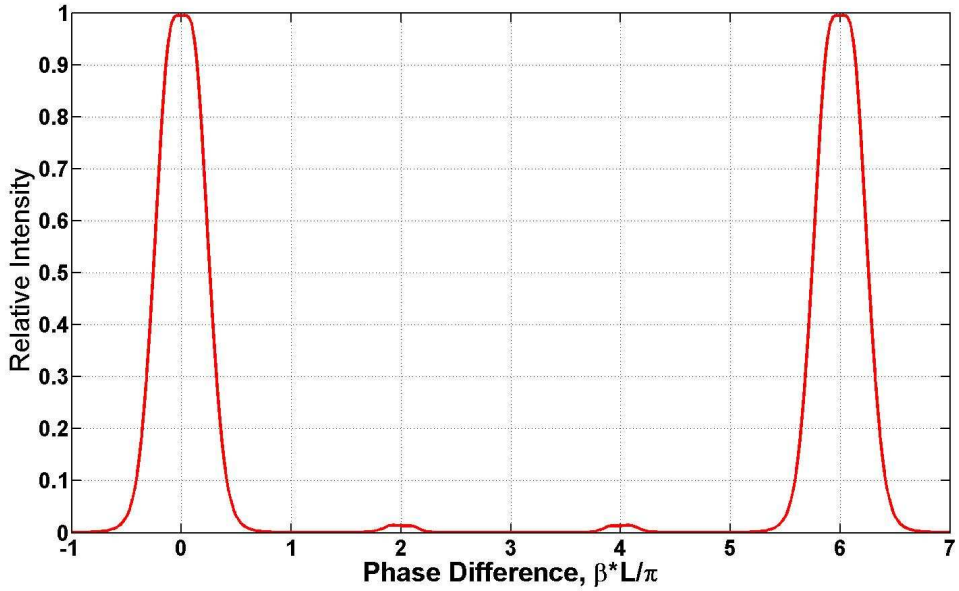

Figure continued on next page

D

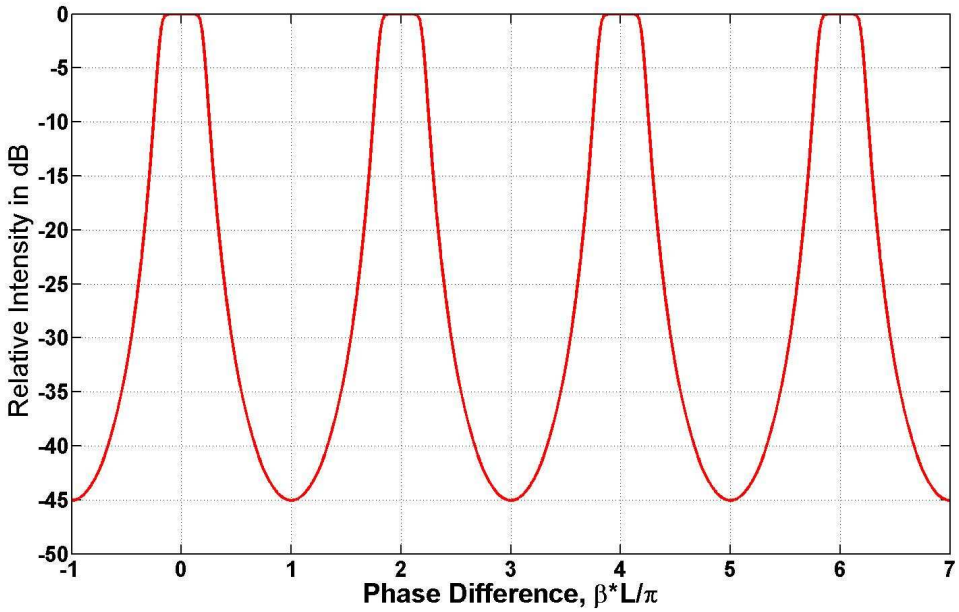

E

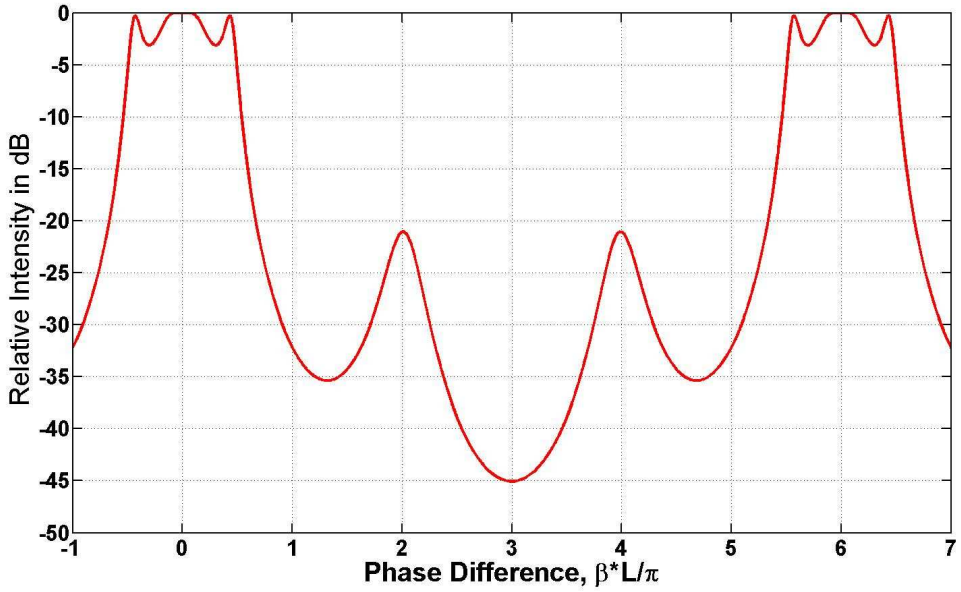

Figure continued on next page

F

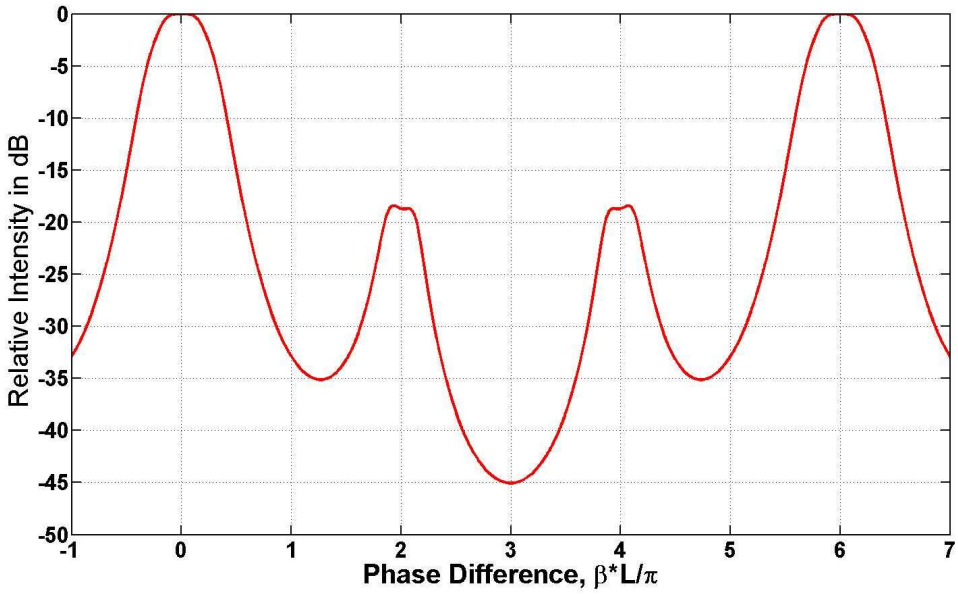

Fig 4.7 *Transfer functions of a four ring resonator with* $r_0 = 0.58$, $r_1 = 0.91$, $r_2 = 0.94$, $r_3 = 0.88$, $r_4 = 0.52$ *and ring circumferences are in the ratio of 1:3. These transfer functions are displayed in both linear units and in decibels. Curves A, B and C are plotted in linear units. Curves D, E and F are the same but plotted in decibels. The ring configurations are: A and D: "equal ring circumferences", B and E: "E" of Fig 4.3, C and F: "B" of Fig 4.3.*

What is important about Figure 4.7 is that the greatest of the side bands is around 20 dB less than the main peak which is much better than with ring circumference ratios of 9:10 (in Fig 4.6), also, the subsidiary peaks of Figure 4.5 and Figure 4.6 are very lower in this configuration.

The simulations performed provide evidence that a circumference ratio of 1:2, which means that the circumferences of the larger rings are twice those of the smaller ones, is a very good configuration for a four-ring resonator. They provide the best result of our simulations. It could probably be improved by spending much more time working on this subject.

A revealing fact is that in configuration E of Figure 4.3, the peaks contain three small sub-peaks at their top and they can become relatively large (cf Figure 4.7 and Figure 4.8). Also, its sideband suppression ratio is 23.5 dB with a ring circumference ratio of 1:2 (as shown in Figure 4.8), which is the best of all the possible symmetries that we have tested.

A

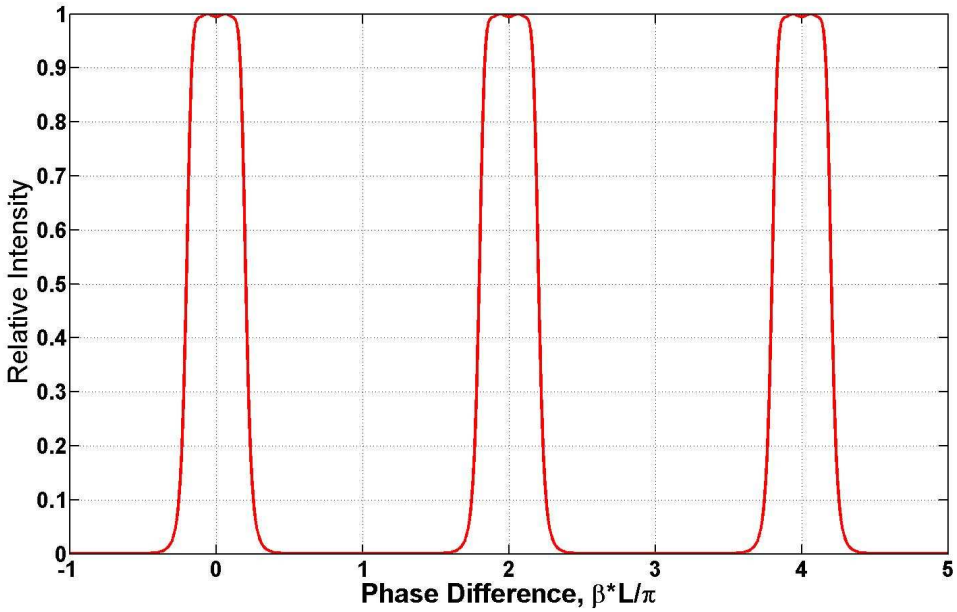

B

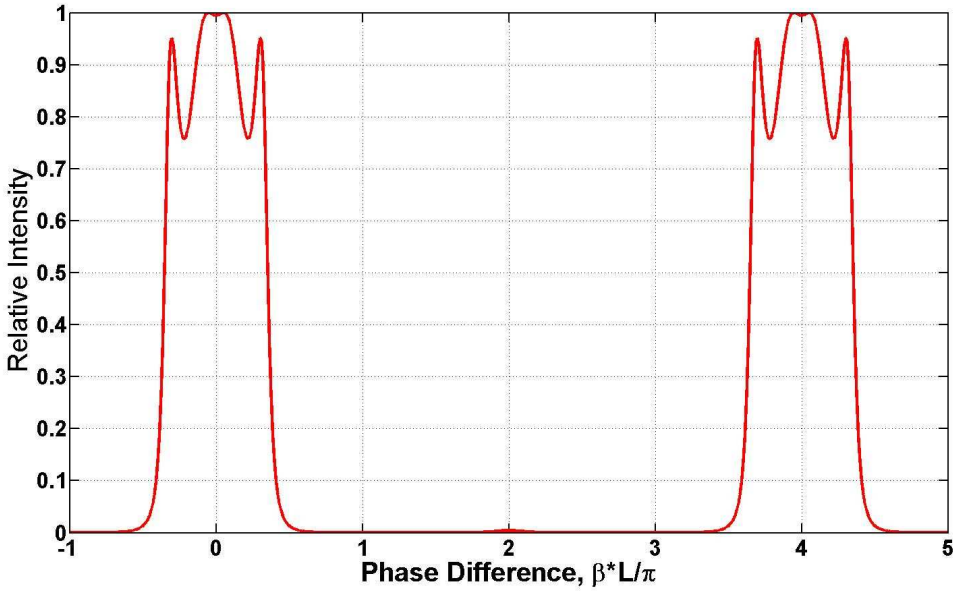

Figure continued on the next page

C

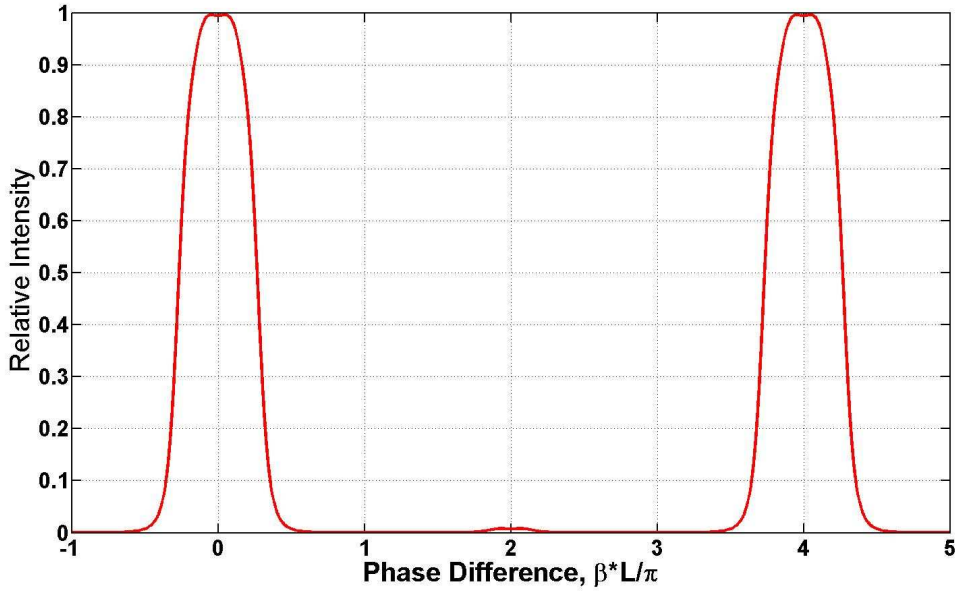

D

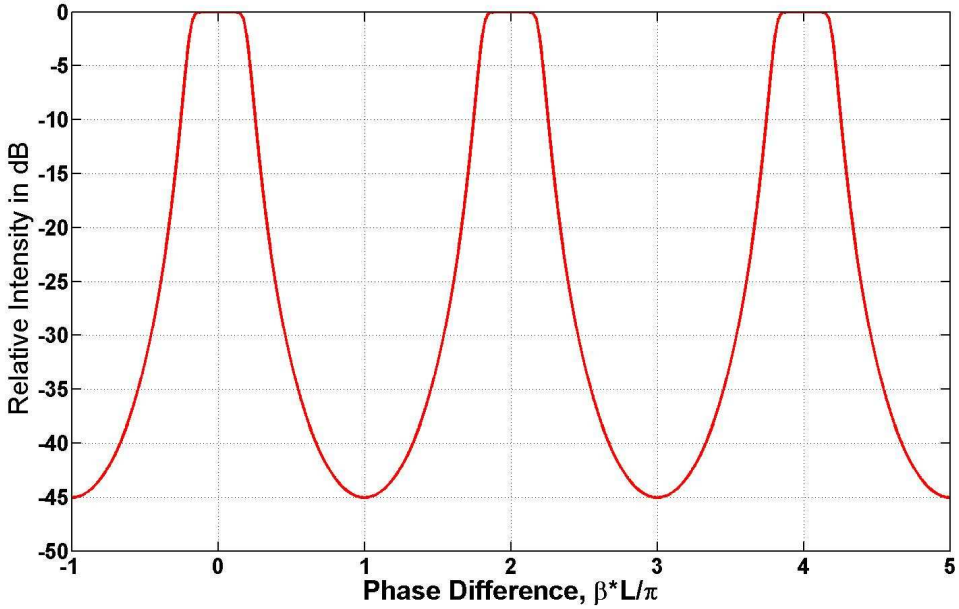

Figure continued on the nexte page

E

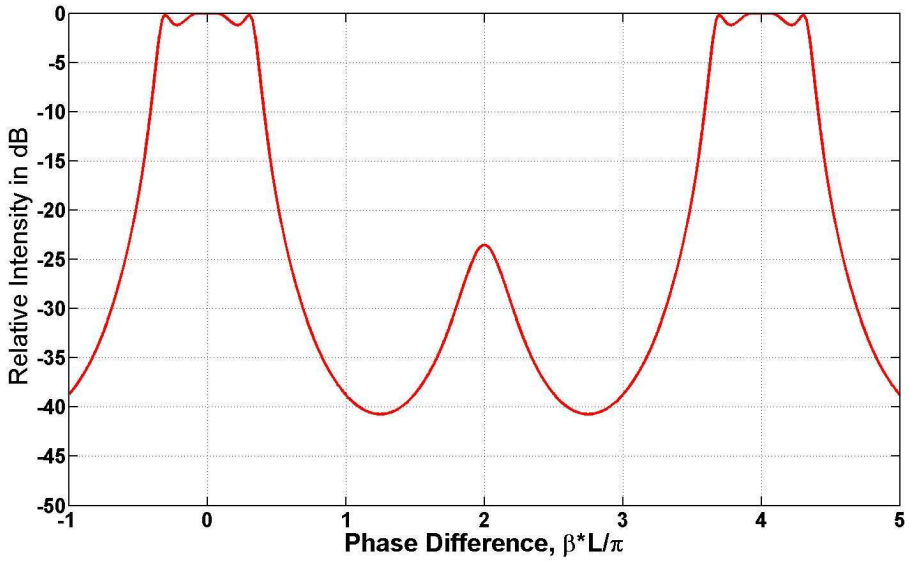

F

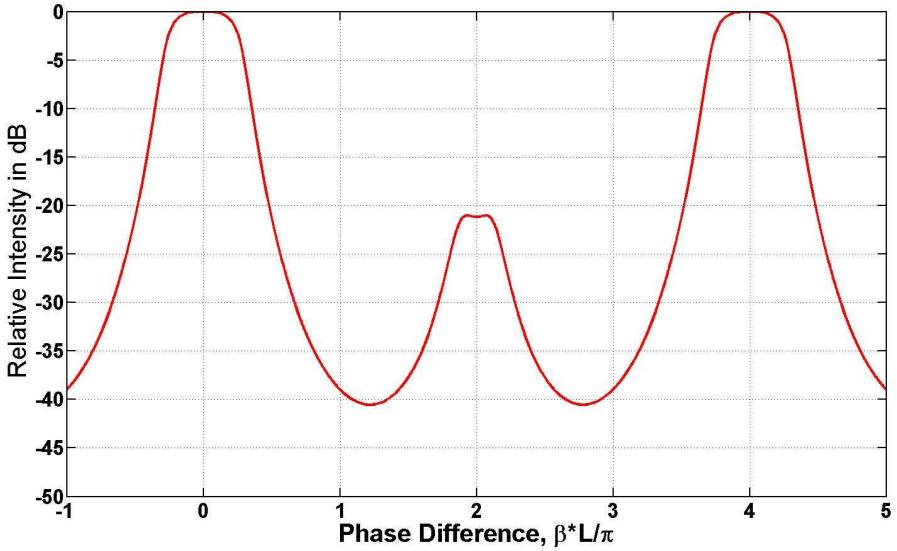

Fig 4.8 *Transfer function of a four ring resonator with $r_0 = 0.5$, $r_1 = 0.91$, $r_2 = 0.94$, $r_3 = 0.88$ and $r_4 = 0.52$. Ring circumferences ratio is of 1:2. These transfer functions are displayed in both linear units and in decibels. Curves A, B and C are plotted in linear units. Curves D, E and F are the sames but plotted in decibels. The ring configurations are: A and D: "equal ring circumferences", B and E: "E" of Figure 4.3, C and F: "B" of Figure 4.3.*

4.4 Study of three-ring resonators

We now study the Vernier effect with a three-ring resonator. This is of interest because (a) it is a simpler structure than a four-ring resonator and thus more easily fabricated and (b) it is the simplest structure that allows us to explore the possibilities of three different circumferences. It is particularly flexible because it is possible to choose the periodicity of the super resonance by selecting the values of circumference of each ring.

In the kind of resonator of Figure 4.9, there are four couplers. Each one has an effective reflectance R. This reflectance is correlated to the coupling ratio K by the formula: $K = 1 - R^2$. The coupling ratios of the inner couplers are equal and the outer couplers' are equal too. In this report, the outer couplers' coupling ratios are K_a and the inner couplers ones are K_b.

We explain how we can set the periodicity by modifying the ring circumferences. There is a peak (it can be a very small one, but it exists) each every 2π of phase difference, in exactly the same manner as a three-ring resonator with equal ring circumferences. If, for example, the three ring circumferences are in the ratio of 4:1:8, there will be a "super resonance" with a peak every two periods of 2 π and also every 8 periods of 2 π. Obviously, the peaks that appeared every 8 periods are very much greater than the others because each of the three rings gives its contribution. An illustration of this phenomenon is presented in Figure 4.10.

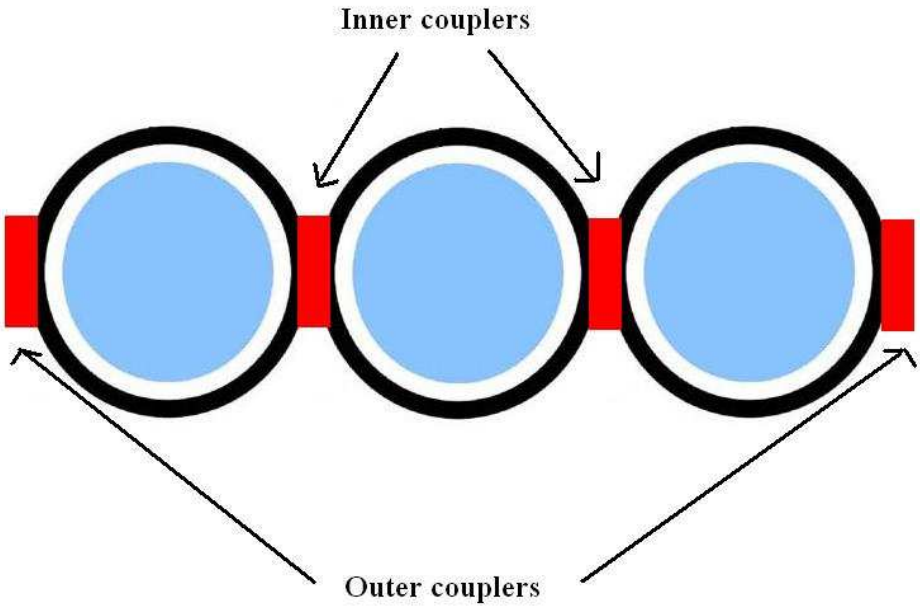

Fig 4.9 *Illustration of a three-ring resonator.*

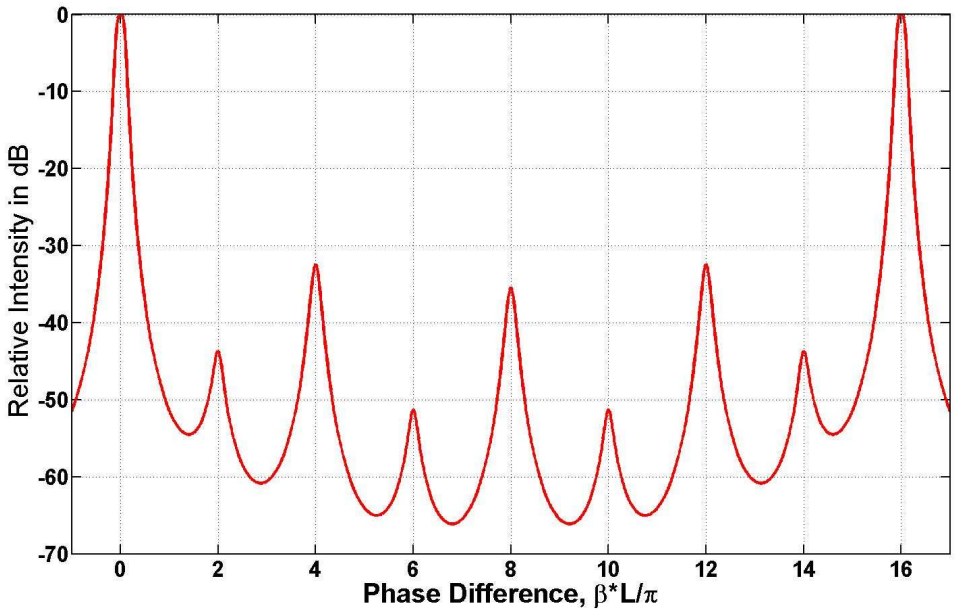

Fig 4.10 *Transfer function of a three-ring resonator with ring circumference ratio 4:1:8 and with K_a=0.45 and K_b=0.005.*

The design of filter to which Figure 4.10 refers is very adaptive and it could provide good characteristics, such as a high sideband suppression ratio and a well shaped transfer function. The peaks can be very close to a "box like" filter and very narrow if the reflection coefficients are appropriately chosen. Using this ring configuration, the reflection coefficients are simple to set: the one for the outer couplers, K_a must be the greatest possible and the inner coupler reflection coefficients K_B must be the smallest possible to have the best sideband suppression. Consequently, the filter with the best sideband suppression has couplers with extreme values. This kind of coupler can be made but it tends to be expensive and have a low production yield.

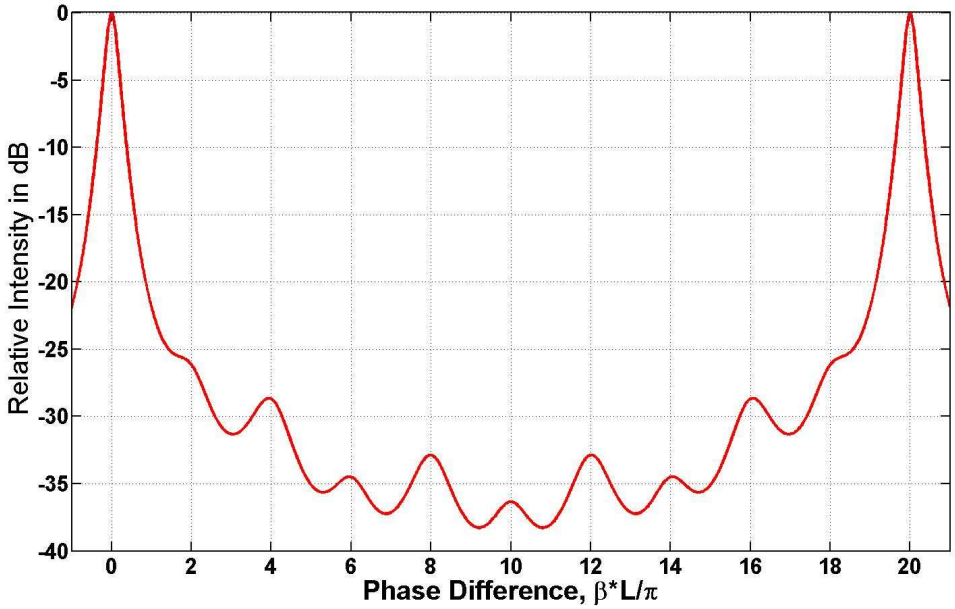

Fig 4.11 *Transfer function of a three ring resonator with K_a=0.97 and K_b=0.03 and ring circumference ratio is 5:1:10.*

Fortunately, it is possible to design filters with good characteristics in which the couplers have ratios that are more easily fabricated. As we can see on Figure 4.11, nearly acceptable filters can be designed using more easily produced couplers. Nevertheless, it is revealing to visualize the best transfer function we could have, even if it is really expensive to manufacture and it is shown in Figure 4.12. We could consider it as the "almost-ideal" filter of this configuration.

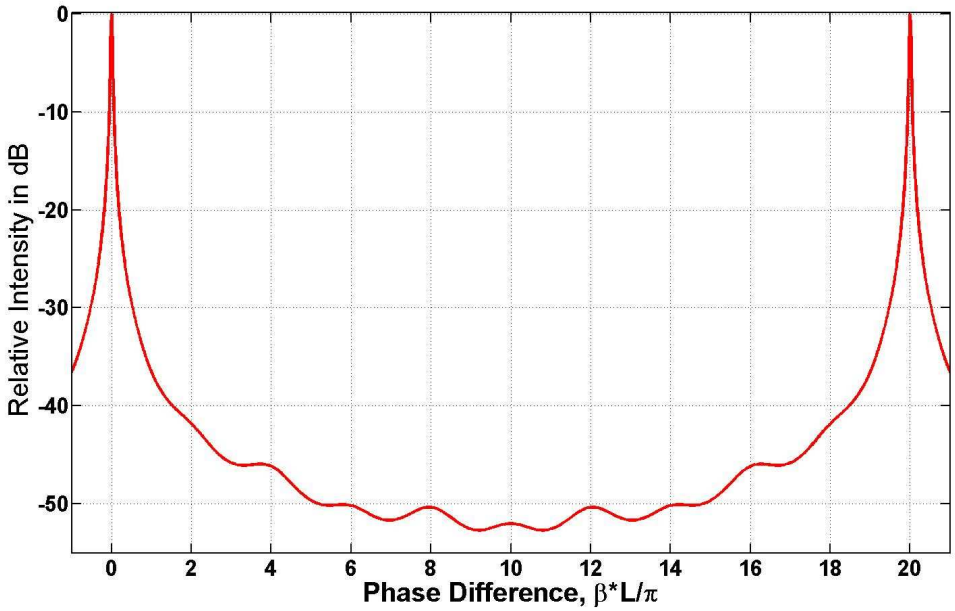

Fig 4.12 *Transfer function of a three-ring resonator with K_a=0.995 and K_b=0.005. The ring circumference ratio is 5:1:10. The vertical axis is in decibels.*

One means to improve the depth of modulation of the filter's transfer function is to set two of the ring circumferences to be equal. An example is illustrated in Figure 4.13. In this specific case, we do not have three levels of peaks (cf Figure 4.10) but only two. Moreover, it is still possible to choose the periodicity of the filter by setting the circumference of the two rings to be equal size.

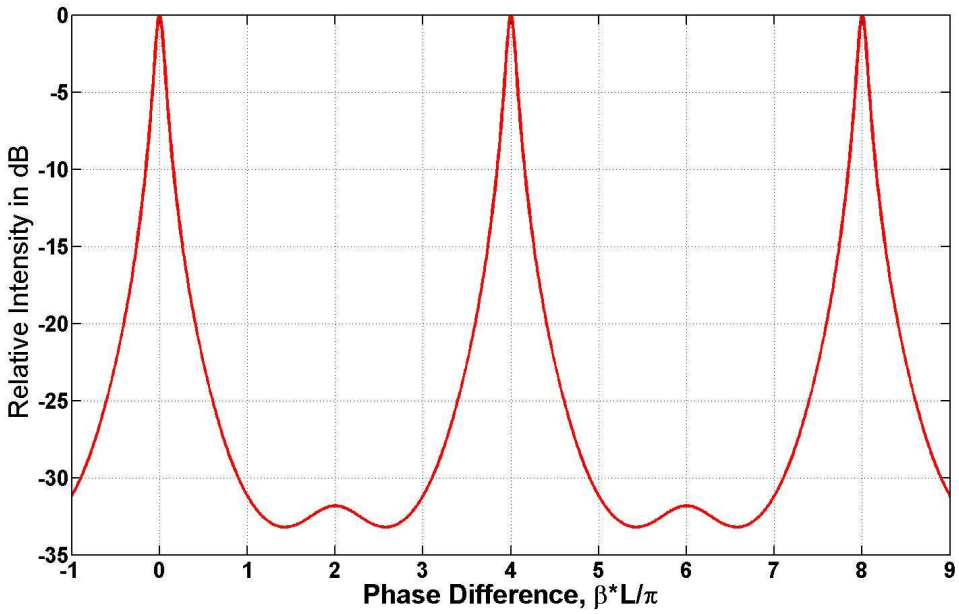

Fig 4.13 *Transfer function of a three ring resonator with K_a=0.95 and K_b=0.05 and ring circumferences of 1:1:2.*

Figure 4.13 allows us to visualize the filter of this configuration with the best depth of modulation. It provides evidence that such filters can provide very good transfer functions. In Figure 4.14 we plot a transfer function with three rings of the same circumferences as Figure 4.13 (ratio of 1:1:2) but we use more extreme values of the coupler ratios. Clearly, the peaks are very narrow and the depth of modulation, which exceeds 50 dB, is likely to be appropriate for many applications. Furthermore, there are no sidebands evident from the logarithmic plot. Unfortunately, the unresolved question is whether such coupling ratios can realistically achieved with acceptable production yields.

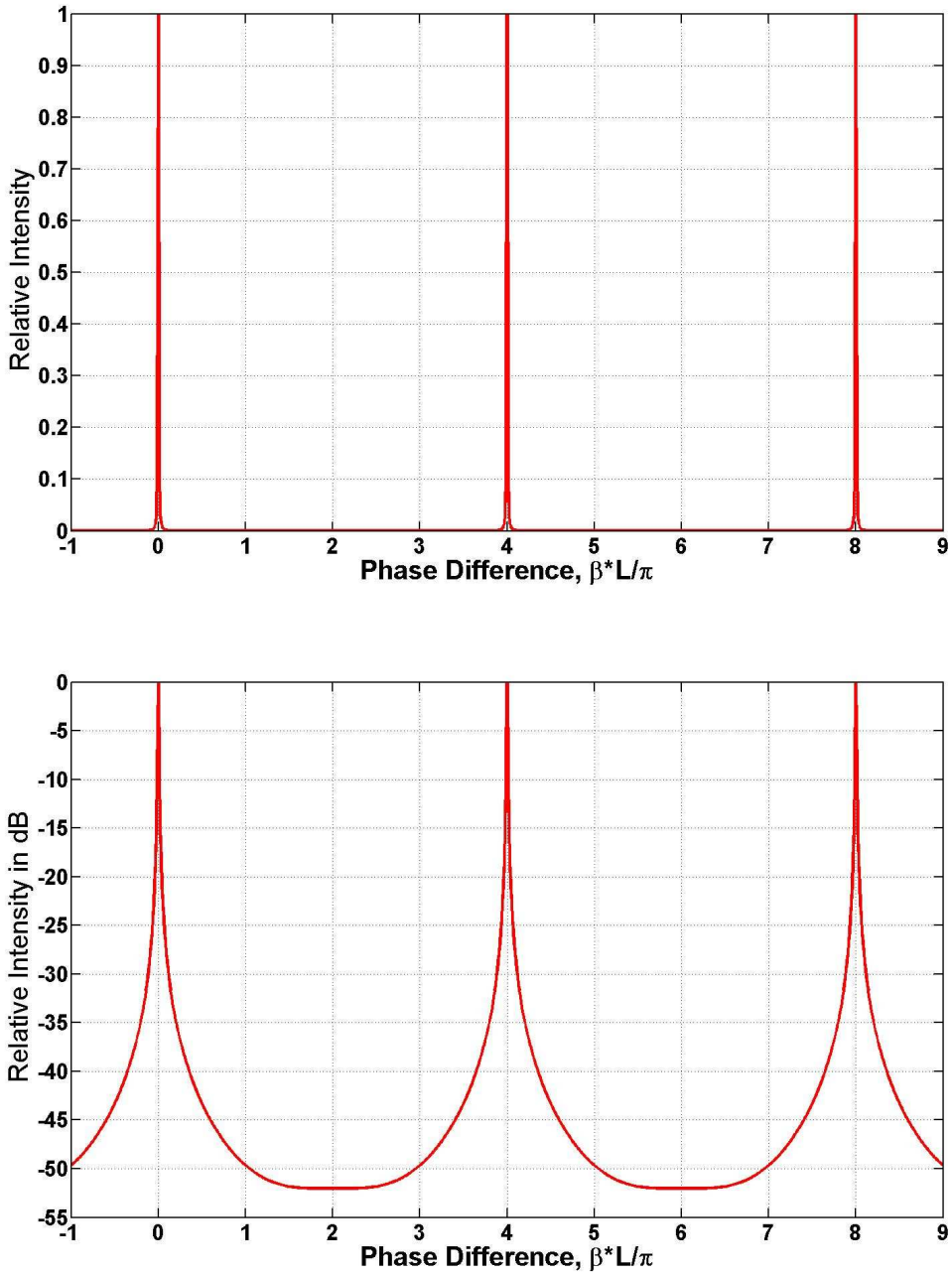

Fig 4.14 *Transfer function of a three-ring resonator. In linear and decibel units. With K_a=0.995 and K_b=0.005. The ring circumferences are in the ratio of 1:1:2. The linear curve is displayed here to show how extremely narrow the peaks are in this case.*

We have seen in this chapter about the Vernier effect that the phenomenon of super resonance can greatly help in the design of optical filters. There are many parameters to adjust. As we have shown, achieving the necessary coupling ratios and ring circumferences is challenging and is an issue to be addressed by specialists in design, fabrication and production technologies.

5 N-Ring Resonators

5.1 Introduction

The purpose of this chapter is to design a ring resonator filter consisting of N coupled rings with the same circumference. At the beginning we tried to continue the work chapter 4 and 5 of Elshoff and Rautenberg; our aim was to extend the formulations made for two or three ring resonators. To do that, the best way is to use "diagonal decomposition", which is a technique for raising a matrix to a power. They obtained encouraging results, but it appears that the derivation of the equations was much more complicated and longer than we had expected. Moreover, as they noted, there is an ever-present possibility of algebraic mistakes. Therefore, we decided to use a numerical technique to design the N-ring transfer function.

In order to calculate the transfer function for an N-ring resonator we need a repetition of the coupler ratios. We have therefore used two kinds of symmetry and thanks to the symmetry we can make some mathematical simplifications and thus reduce the computation time.

5.2 Matlab Function

As we explain in Chapter 3 we used a Matlab program to calculate the complicated transfer function. The program we used for calculating and plotting the N-ring resonator transfer function has eleven parameters; they are defined in Table 5.1.

Parameters	Details	Dimension
N	Number of Rings	Dimensionless
L	Circumference of the Rings	m
Alpha	Bending, scattering and absorption loss coefficient	m^{-1}
Depth	Minimum depth of modulation	dB
Precision	Precision of the computing compilation	Dimensionless
Precision_R	Precision of the coupling ratio	Dimensionless
Precision_I	Minimum variation at the top of the transfer function (see Figure 5.1)	dB
FinMin	Minimum finesse	dB
FinMax	Maximum finesse	dB
M	Number of points to plot the transfer function	Dimensionless
Symmetry	Category of symmetry between the coupling ratios	Dimensionless

Table 5.1 *Parameters of the Matlab function which calculates and plots the transfer function of an N-Ring resonator filter.*

The parameter Precision_i defines the size of the relative intensity variations which are on the top of the transfer function and they are illustrated in Figure 5.1.

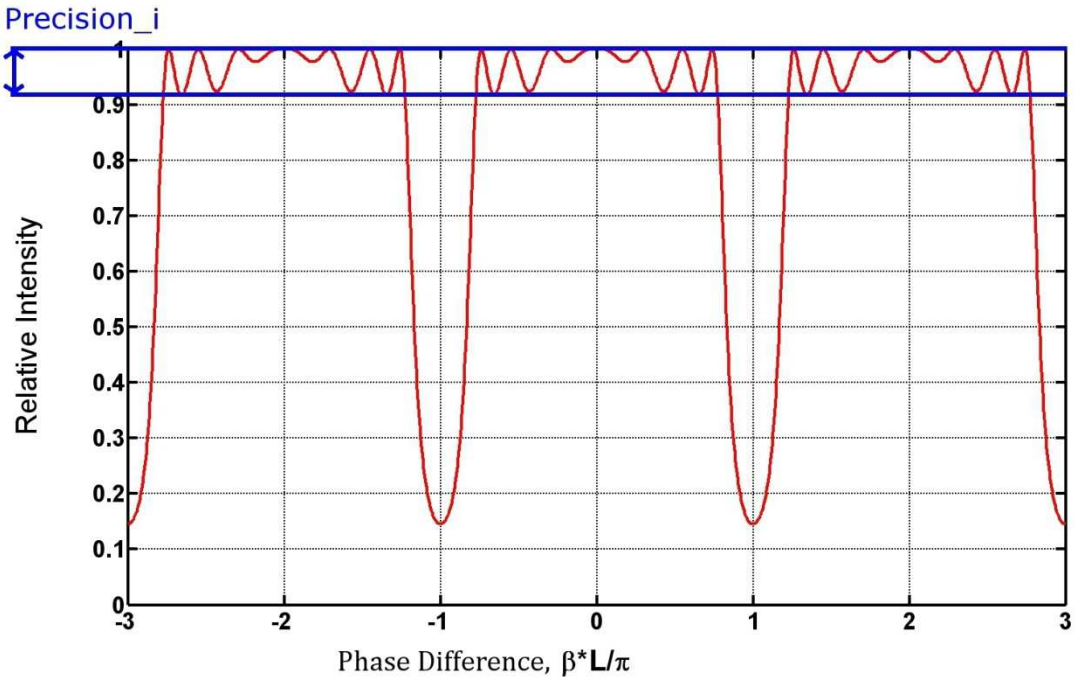

Fig 5.1 *Example of the use of the parameter precision_i. The curve is the relative intensity of a resonator with N = 8 rings, the first category of symmetry with $r_0 = 0.1$, $r_1 = 0.2$ and $r_2 = 0.05$.*

The function calculates a relative intensity for each combination of effective reflectances. For example, if there are three effective reflectances, r_0, r_1 and r_2, and the parameter precision_R is 0.05, there will be 19 possible values for each effective reflectance (from 0.05 to 0.95) and therefore 19^3 combinations. The function tests each transfer function to check if it respects all the parameters; if it is the case then the relative intensity will be plotted.

5.3 First category of symmetry: Formulation

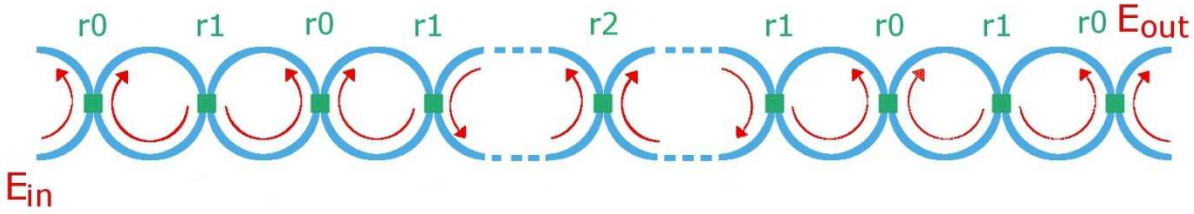

Fig 5.2 *N-Ring resonator with the first symmetry category. The arrows represent the direction of the light, which alternates clockwise and counter-clockwise. In green are the couplers with their coupling ratios. The dotted waveguides show that we can add an arbitrary number of ring pairs.*

It was established in Section 2.5 that a matrix formulation exists for an array of coupled rings, as we can see in Equation (5.1) [7].

$$\begin{bmatrix} E_{\text{in Alternative}} \\ E_{\text{out}} \end{bmatrix} = M \cdot \begin{bmatrix} E_{\text{in}} \\ E_{\text{out Alternative}} \end{bmatrix} \qquad (5.1)$$

To obtain the transfer function we need to calculate $\frac{E_{out}}{E_{in}}$. We can decompose the matrix M as

$$M = M_k \cdot M_{k-1} \cdot [\cdots] \cdot M_{k/2} \cdot [\cdots] \cdot M_2 \cdot M_1 \qquad (5.2)$$

An important feature of Equation (5.2) is the ordering of the matrices. Light propagates through the compound resonator, entering at the left and exiting on the right. However, the matrix M_1 is on the right and the subscripts increase towards the left, where the last one is M_K. As in all matrix multiplications, it is important to observe the order. The right-to-left order also applies in other compound filter formulations in optics, electronics and microwaves.

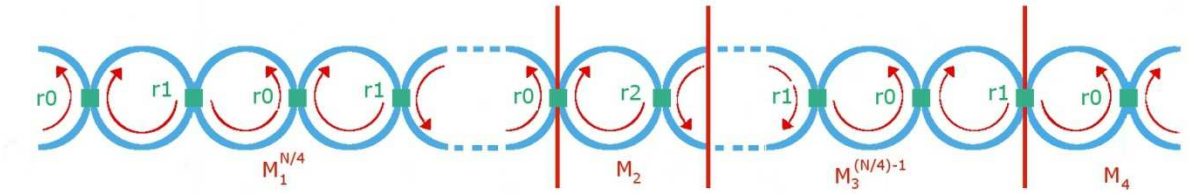

Fig 5.3 *Distribution of the different matrices on an N-Ring resonator with the first symmetry category.*

Thanks to the symmetry we can write Equation (5.2) in another way, as stated in Equation (5.3)

$$M = M_{14} \cdot M_{13}^{\left(\frac{N}{4}\right)-1} \cdot M_{12} \cdot M_{11}^{\frac{N}{4}} \qquad (5.3)$$

The last thing to do is to determine the four constituent matrices in Equation (5.3). We can consider the first one as shown in Figure 5.4.

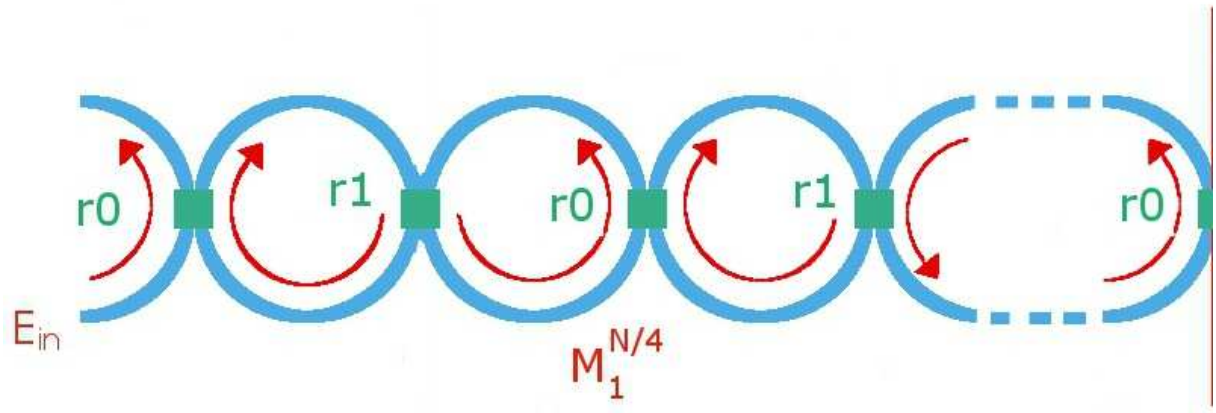

Fig 5.4 *First group of rings of an N-Ring resonator using the first symmetry category.*

The greatest problem is that we cannot perform the calculation by raising the matrix of single ring resonator to the power of N. First, it is because there are two different coupling ratios in this part of the N-ring resonator and second, the direction of light within the rings alternates clockwise and counter-clockwise. Therefore, we need to regroup pairs of rings, as shown in Figure 5.4, so we need to formulate a matrix of a two ring resonator.

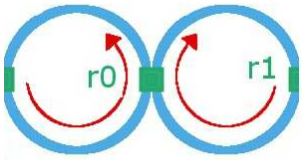

Fig 5.5 *Two-ring resonator showing the opposite directions of the propagating light.*

We have to multiply a matrix to formulate a pair of rings, in which the light is travelling clockwise in one and counter-clockwise in the other. This is done in Equation (5.4).

$$M_{11} = \begin{bmatrix} \left(\frac{r_1}{t_1}\right)\cdot e^{\delta/2} & \left(\frac{t_1^2 - r_1^2}{t_1}\right)\cdot e^{\delta/2} \\ \left(\frac{1}{t_1}\right)\cdot e^{-\delta/2} & \left(\frac{r_1}{t_1}\right)\cdot e^{-\delta/2} \end{bmatrix} \cdot \begin{bmatrix} -\left(\frac{r_0}{t_0}\right)\cdot e^{-\delta/2} & \left(\frac{1}{t_0}\right)\cdot e^{-\delta/2} \\ \left(\frac{t_0^2 - r_0^2}{t_0}\right)\cdot e^{\delta/2} & \left(\frac{r_0}{t_0}\right)\cdot e^{\delta/2} \end{bmatrix}$$

$$= \begin{bmatrix} \frac{-r_0 * r_1 + (t_0^2 - r_0^2) * (t_1^2 - r_1^2)\cdot e^{\delta}}{t_0 * t_1} & \frac{r_1 + r_0 * (t_1^2 - r_1^2)\cdot e^{\delta}}{t_0 * t_1} \\ \frac{-r_1 * (t_0^2 - r_0^2) - r_0 \cdot e^{-\delta}}{t_0 * t_1} & \frac{-(r_0 * r_1) + e^{-\delta}}{t_0 * t_1} \end{bmatrix} \quad (5.4)$$

Now we must raise the matrix in Equation (5.4) to the power of N/4. Then we need to formulate the central matrix, this is with the effective reflectance r_2, as depicted in Figure 5.6.

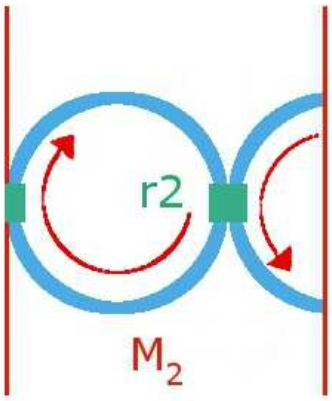

Fig 5.6 *Central ring of an N-Ring resonator using the first kind of symmetry.*

We require a matrix formulation of a single ring resonator when the light circulates in a clockwise direction and it is given by Equation (5.5).

$$M_{12} = \begin{bmatrix} -\left(\frac{r_2}{t_2}\right) \cdot e^{-\delta/2} & \left(\frac{1}{t_2}\right) \cdot e^{-\delta/2} \\ \left(\frac{t_2^2 - r_2^2}{t_2}\right) \cdot e^{\delta/2} & \left(\frac{r_2}{t_2}\right) \cdot e^{\delta/2} \end{bmatrix} \qquad (5.5)$$

So now for the followings rings we cannot raise the transfer matrix of a two ring resonator to the power of N/4 but if we separate them for the last ring we can raise the transfer matrix of a two ring resonator to the power of (N/4)-1.

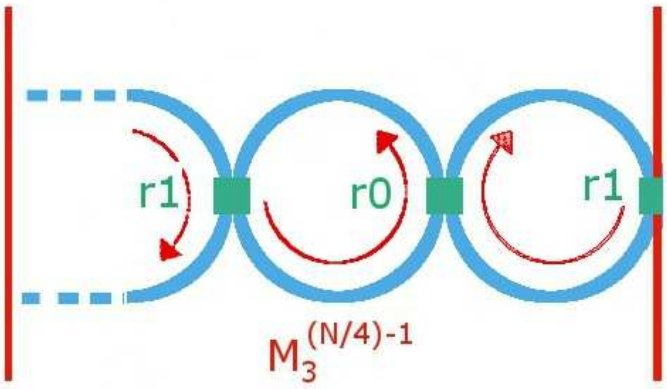

Fig 5.7 *Part of an N-Ring resonator using the first symmetry category.*

The transfer matrix of the two-ring resonator, M_{13} is very close to the matrix M_{11} from Equation (5.4); only the order of the coupler ratios and the direction of the light are different.

$$M_{13} = \begin{bmatrix} \frac{-r_0 * r_1 + e^{-\delta}}{t_0 * t_1} & \frac{-r_0 * (t_1^2 - r_1^2) - r_1 \cdot e^{\delta}}{t_0 * t_1} \\ \frac{r_0 + r_1 * (t_0^2 - r_0^2) \cdot e^{-\delta}}{t_0 * t_1} & \frac{-(r_0 * r_1) + (t_0^2 - r_0^2) * (t_1^2 - r_1^2) \cdot e^{-\delta}}{t_0 * t_1} \end{bmatrix} \quad (5.6)$$

Now we can raise this matrix M_{13} to the power of (N/4)-1 to obtain the matrix formulation of this part of the N-Ring resonator. However, we still need to find the matrix formulation of the last ring, details of which are on Figure 5.8.

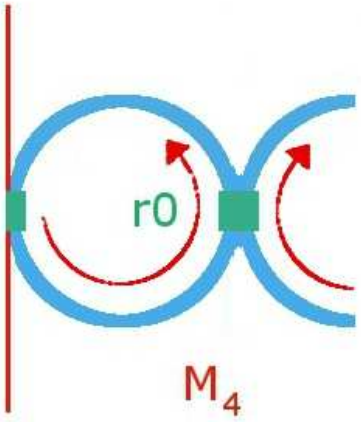

Fig 5.8 *Last ring and output waveguides of an N-Ring resonator using the first kind of symmetry.*

To formulate the last ring we must multiply the matrix of a single ring resonator with the matrix formulation for a coupler with effective reflectance r_0.

$$M_{14} = \begin{bmatrix} \frac{1}{t_0} & -\frac{r_0}{t_0} \\ \frac{r_0}{t_0} & \frac{t_0^2 - r_0^2}{t_0} \end{bmatrix} \cdot \begin{bmatrix} \left(\frac{r_1}{t_1}\right) \cdot e^{\delta/2} & \left(\frac{t_1^2 - r_1^2}{t_1}\right) \cdot e^{\delta/2} \\ \left(\frac{1}{t_1}\right) \cdot e^{-\delta/2} & \left(\frac{r_1}{t_1}\right) \cdot e^{-\delta/2} \end{bmatrix} \quad (5.7)$$

Then, we have

$$M_{14} = \begin{bmatrix} \left(\frac{r_1}{t_1 * t_0}\right) \cdot e^{\delta/2} - \left(\frac{r_0}{t_1 * t_0}\right) \cdot e^{-\delta/2} & \left(\frac{t_1^2 - r_1^2}{t_1 * t_0}\right) \cdot e^{\delta/2} - \left(\frac{r_0 * r_1}{t_1 * t_0}\right) \cdot e^{-\delta/2} \\ \left(\frac{r_0 * r_1}{t_1 * t_0}\right) \cdot e^{\delta/2} + \left(\frac{t_0^2 - r_0^2}{t_1 * t_0}\right) \cdot e^{-\delta/2} & \left(\frac{r_0 * (t_1^2 - r_1^2)}{t_1 * t_0}\right) \cdot e^{\delta/2} - \left(\frac{r_1 * (t_0^2 - r_0^2)}{t_1 * t_0}\right) \cdot e^{-\delta/2} \end{bmatrix} \quad (5.8)$$

Now we must multiply the matrices stated in Equations (5.4), (5.5), (5.6) and (5.8) to obtain the matrix formulation of an N-Ring resonator with the first kind of symmetry. We can consider the product matrix from Equation (5.3) as:

$$M = \begin{bmatrix} q_{11} & q_{12} \\ q_{21} & q_{22} \end{bmatrix} \tag{5.9}$$

$$\begin{bmatrix} E_{\text{in Alternative}} \\ E_{\text{out}} \end{bmatrix} = \begin{bmatrix} q_{11} & q_{12} \\ q_{21} & q_{22} \end{bmatrix} \cdot \begin{bmatrix} E_{\text{in}} \\ E_{\text{out Alternative}} \end{bmatrix} \tag{5.10}$$

So the amplitude function is:

$$\frac{E_{out}}{E_{in}} = \frac{q_{22} \cdot q_{11} - q_{12} \cdot q_{21}}{q_{22}} \tag{5.11}$$

The relative intensity is obtained by squaring modulus of the amplitude transfer function.

$$\frac{I_{out}}{I_{in}} = \left| \frac{E_{out}}{E_{in}} \right|^2 \tag{5.12}$$

5.4 First category of symmetry: Results

Elshoff and Rautenberg have already plotted the relative intensity of one-, two- and three-ring resonators, so we decide to begin with the transfer function of a 4-ring resonator, as shown in Figures 5.9 and 5.10.

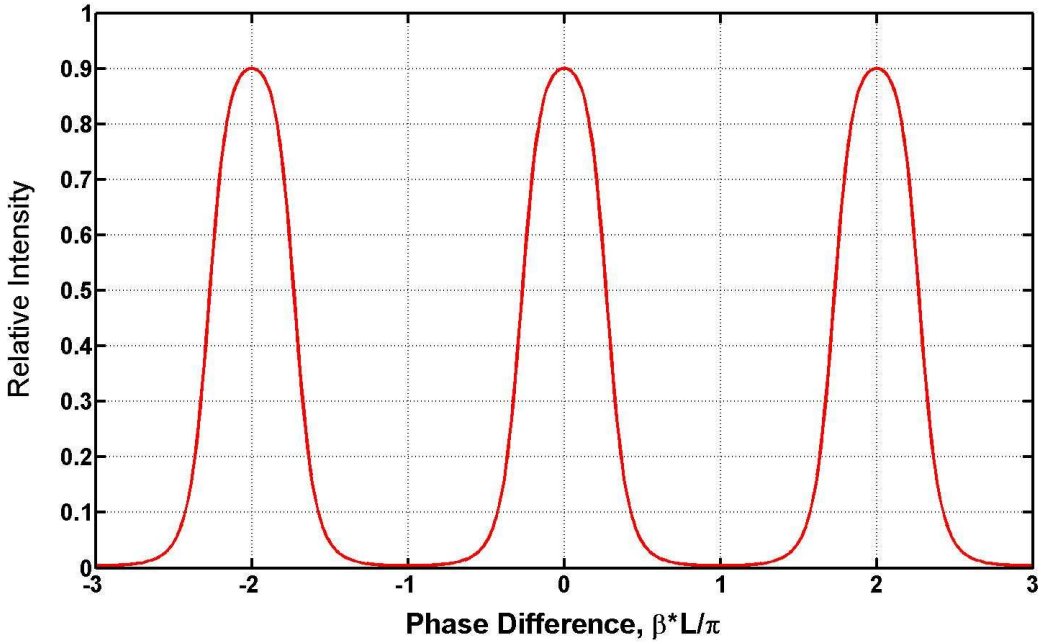

Fig 5.9 *Transfer Function in linear units: Relative intensity of a 4-ring resonator with the first kind of symmetry with r_0 = 0.2, r_1 = 0.65 and r_2 = 0.9. The depth of modulation is 23.8 dB.*

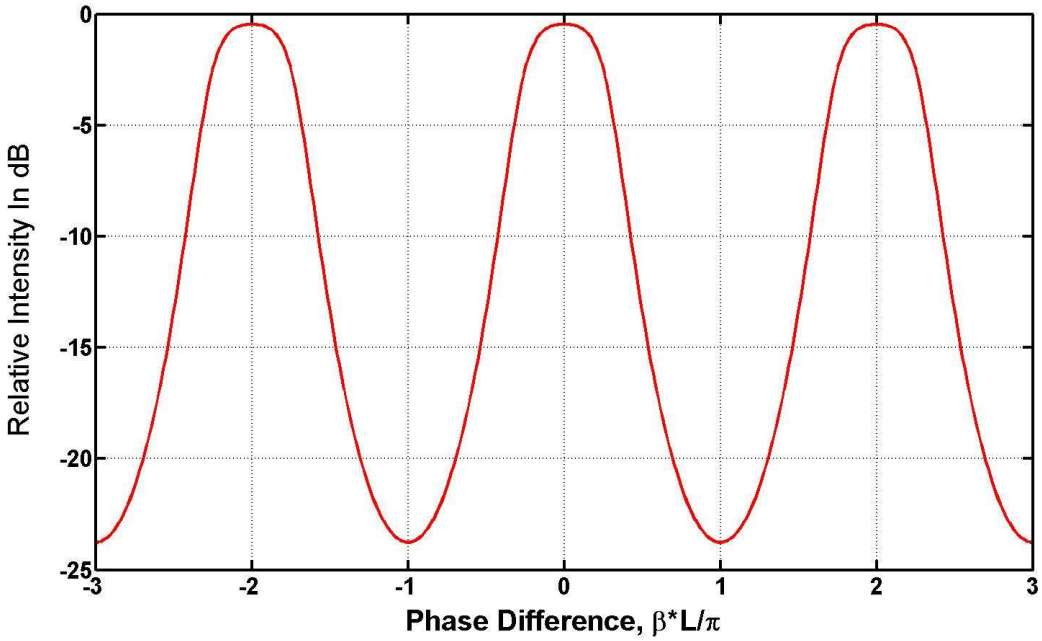

Fig 5.10 *Relative Intensity transfer function in dB of a 4-ring resonator with the first kind of symmetry with r_0 = 0.2, r_1 = 0.65 and r_2 = 0.9. The depth of modulation is of 23.8 dB.*

The resonator is quite encouraging because, as Figures 5.9 and 5.10 illustrate, the depth of modulation is good and its profile is almost a "box-like" function. However, the maximum relative intensity is only 0.9 and, most disturbing, the bandwidth is very large. On the basis of the studies of two- and three-ring resonators reported by Elshoff and Rautenberg [1], it is likely that the peak transmission can be improved beyond what is show in Figure 5.9 but we doubt that it will be possible to reduce the bandwidth significantly. The purpose of this study is to design ring resonators for DWDM filters. With a large bandwidth like that it will be impossible to extract just one DWDM channel.

In order to examine a wider range of possibilities, we have calculated the transfer functions of resonators with N = 8 and 16 rings. The results are plotted in Figures 5.11 to 5.14.

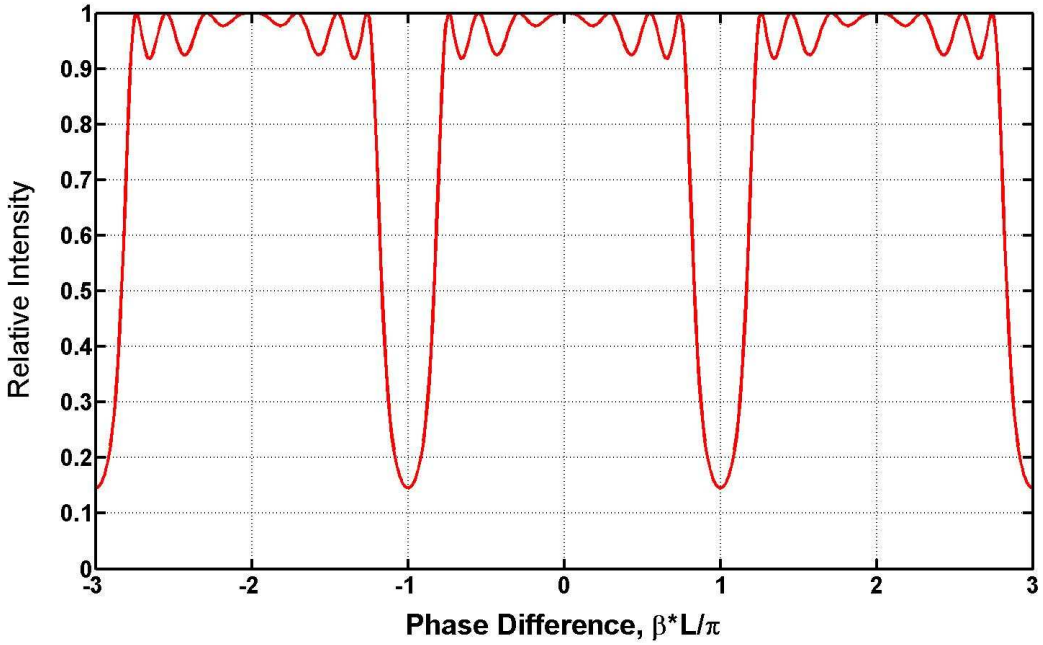

Fig 5.11 *Transfer Function in linear units: Relative intensity of an 8-Ring resonator with the first kind of symmetry with r_0 = 0.15, r_1 = 0.2 and r_2 = 0.2. The depth of modulation is 8.4 dB.*

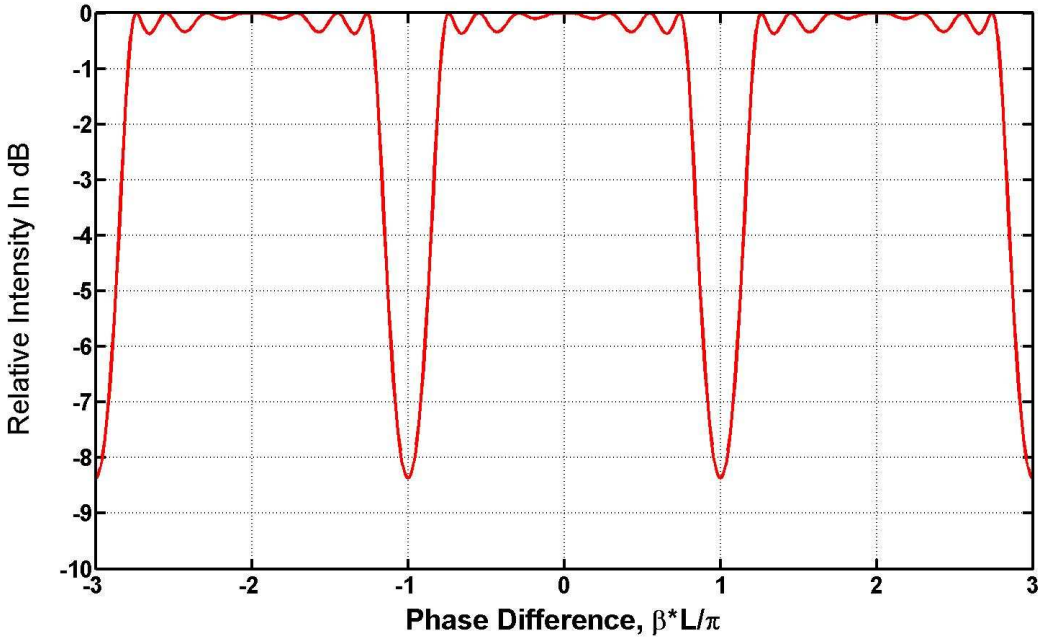

Fig 5.12 *Relative Intensity transfer function in dB of an 8-Ring resonator with the first kind of symmetry with r_0 = 0.15, r_1 = 0.2 and r_2 = 0.2. The depth of modulation is 8.4 dB.*

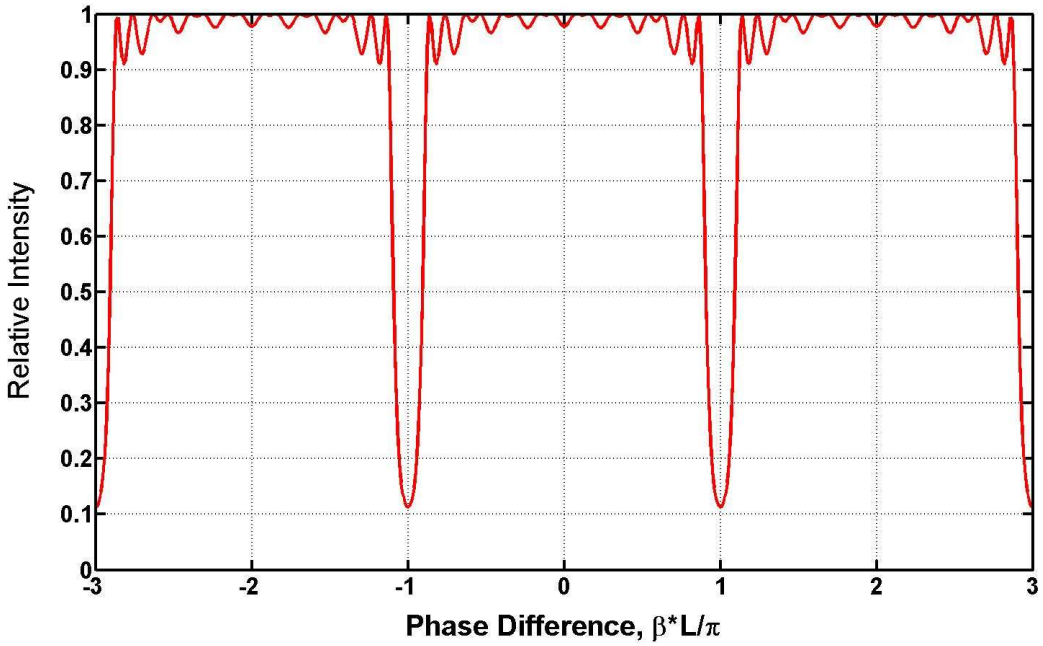

Fig 5.13 *Transfer function in linear units: Relative intensity of a 16-Ring resonator with the first kind of symmetry with r_0 = 0.1, r_1 = 0.1 and r_2 = 0.15. The depth of modulation is 9.5 dB.*

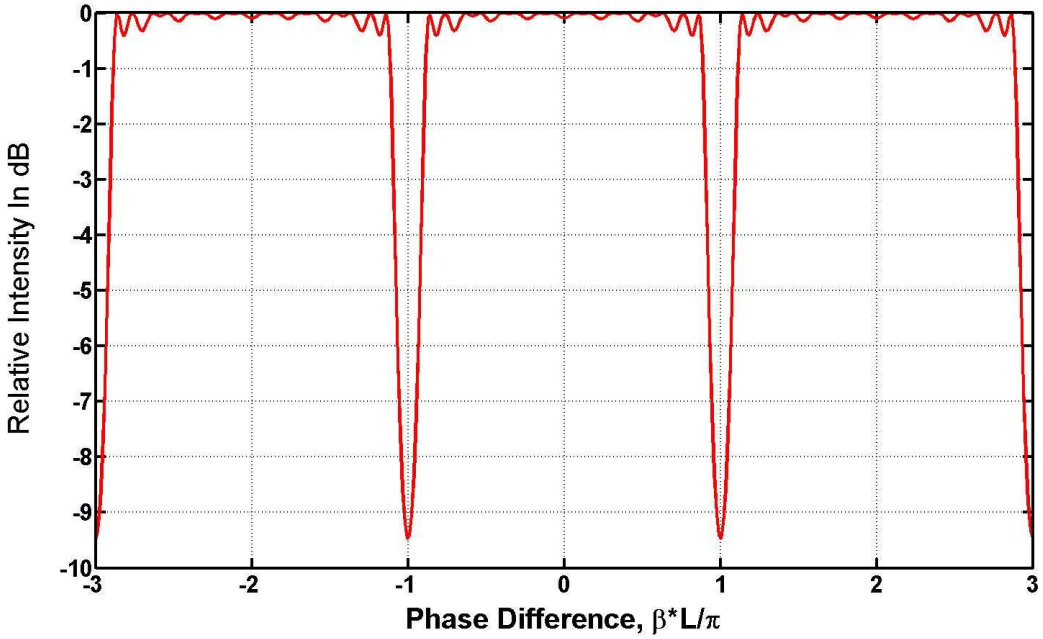

Fig 5.14 *Intensity transfer function in dB of a16-Ring resonator with the first kind of symmetry with r_0 = 0.1, r_1 = 0.1 and r_2 = 0.15. The depth of modulation is 9.5 dB*

The results on Figures 5.11 to 5.14 are quite encouraging because, even if we have not designed a channel passing filter, we have achieved a channel dropping response. On the other hand the depth of modulation is small.

5.5 Second category of symmetry: Formulation

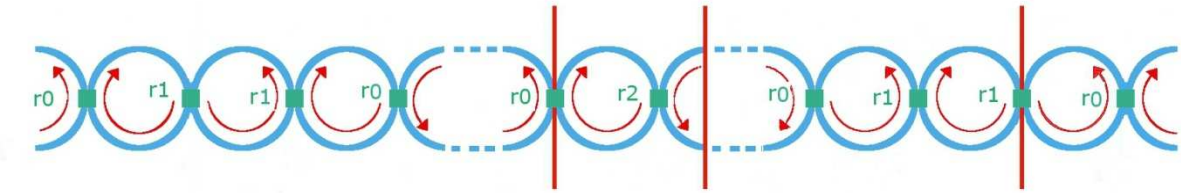

Fig 5.15 *N-Ring resonator with the second kind of symmetry.*

We now examine another ring structure, which is illustrated in Figure 5.15. The principle is the same as first category; the main difference is that instead of raising two matrices to the power of N/4 or (N/4 -1), there are two matrices raised to the power of N/8 or (N/8 -1) but they correspond to the formulation of a four ring resonator.

We can therefore formulate the N-ring resonator as:

$$M = M_{24} \cdot M_{23}^{\left(\frac{N}{8}\right)-1} \cdot M_{22} \cdot M_{21}^{\frac{N}{8}} \qquad (5.13)$$

The first matrix, M_{21}, is the formulation of the first group of four rings. So we can use the matrix M_{11} that we have previously calculated for the first kind of symmetry for the two first rings. The next two rings are very easy to formulate; we just have to swap the coupler ratios in the matrix, and if we multiply these two matrices we have the matrix formulation of the four firsts rings, as illustrated in Figure 5.16.

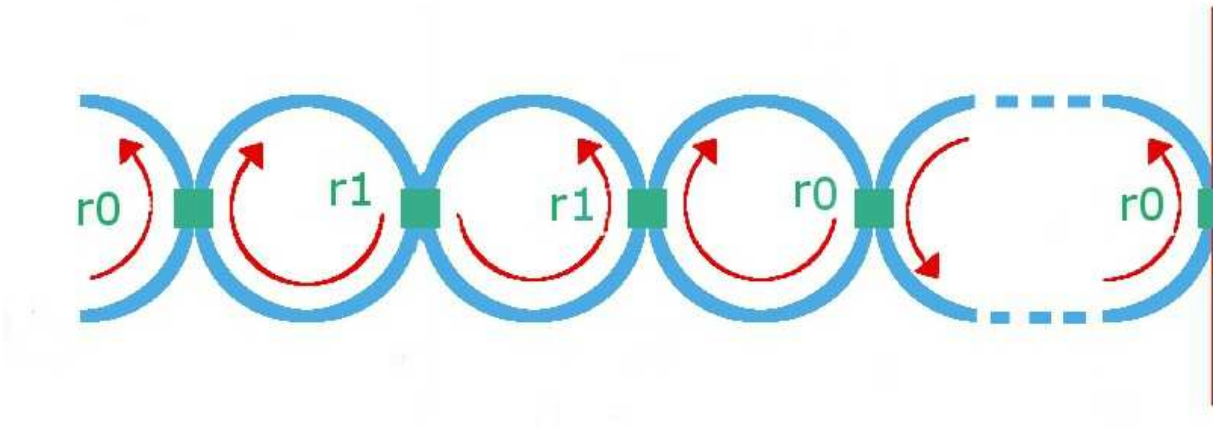

Fig 5.16 *First group of rings of an N-Ring resonator using the second symmetry category.*

The appropriate terms can be substituted into Equation (5.13) to give:

$$M_{21} = \begin{bmatrix} \frac{-r_0 * r_1 + (t_0^2 - r_0^2) * (t_1^2 - r_1^2) \cdot e^{\delta}}{t_0 * t_1} & \frac{r_0 + r_1 * (t_0^2 - r_0^2) \cdot e^{\delta}}{t_0 * t_1} \\ \frac{-r_0 * (t_1^2 - r_1^2) - r_1 \cdot e^{-\delta}}{t_0 * t_1} & \frac{-(r_0 * r_1) + e^{-\delta}}{t_0 * t_1} \end{bmatrix} \cdot M_{11} \quad (5.14)$$

When expanded, we have:

$$M_{21} = \begin{bmatrix} \frac{-r_0*r_1+(t_0^2-r_0^2)*(t_1^2-r_1^2)\cdot e^{\delta}}{t_0*t_1} & \frac{r_0+r_1*(t_0^2-r_0^2)\cdot e^{\delta}}{t_0*t_1} \\ \frac{-r_0*(t_1^2-r_1^2)-r_1\cdot e^{-\delta}}{t_0*t_1} & \frac{-(r_0*r_1)+e^{-\delta}}{t_0*t_1} \end{bmatrix} \cdot \begin{bmatrix} \frac{-r_0*r_1+(t_0^2-r_0^2)*(t_1^2-r_1^2)\cdot e^{\delta}}{t_0*t_1} & \frac{r_1+r_0*(t_1^2-r_1^2)\cdot e^{\delta}}{t_0*t_1} \\ \frac{-r_1*(t_0^2-r_0^2)-r_0\cdot e^{-\delta}}{t_0*t_1} & \frac{-(r_0*r_1)+e^{-\delta}}{t_0*t_1} \end{bmatrix} \quad (5.15)$$

Now we merely have to raise this matrix at the power of N/8.

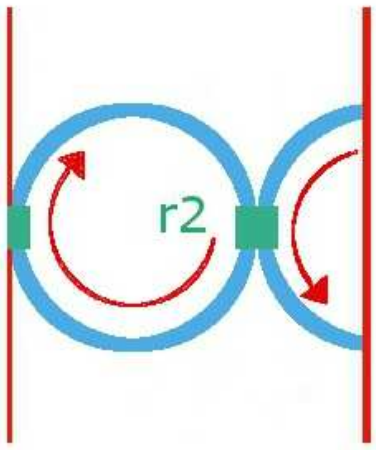

Fig 5.17 *Central ring of an N-Ring resonator using the second symmetry category.*

The matrix M_{22} is exactly the same as M_{12}, as given by Equation (5.5).

$$M_{22} = M_{12} \quad (5.16)$$

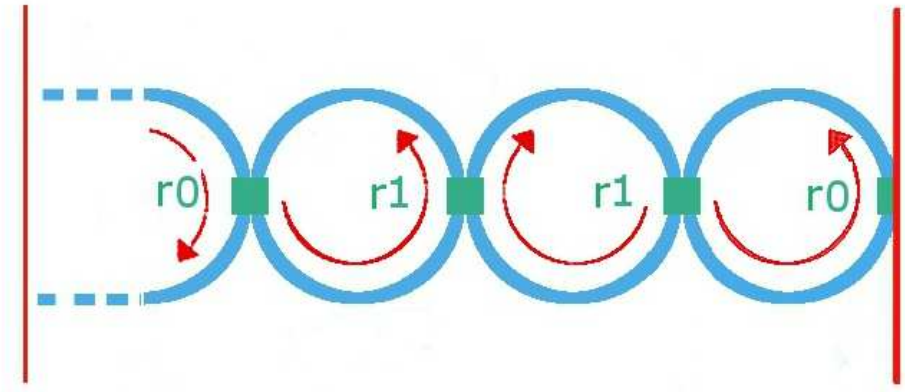

Fig 5.17 *Part of an N-Ring resonator using the second symmetry category.*

For M_{23} we can use the third matrix of the first kind of symmetry, M_{13}. Indeed, we just have to multiply M_{13} by the same matrix as M_{13} but with a simple swapping of effective reflectances.

$$M_{23} = M_{13} \cdot \begin{bmatrix} \frac{-r_0 * r_1 + e^{-\delta}}{t_0 * t_1} & \frac{-r_1 * (t_0^2 - r_0^2) - r_0 \cdot e^{\delta}}{t_0 * t_1} \\ \frac{r_1 + r_0 * (t_1^2 - r_1^2) \cdot e^{-\delta}}{t_0 * t_1} & \frac{-(r_0 * r_1) + (t_0^2 - r_0^2) * (t_1^2 - r_1^2) \cdot e^{-\delta}}{t_0 * t_1} \end{bmatrix} \quad (5.16)$$

$$M_{23} = \begin{bmatrix} \frac{-r_0*r_1+e^{-\delta}}{t_0*t_1} & \frac{-r_0*(t_1^2-r_1^2)-r_1\cdot e^{\delta}}{t_0*t_1} \\ \frac{r_0+r_1*(t_0^2-r_0^2)\cdot e^{-\delta}}{t_0*t_1} & \frac{-(r_0*r_1)+(t_0^2-r_0^2)*(t_1^2-r_1^2)\cdot e^{-\delta}}{t_0*t_1} \end{bmatrix} \cdot \begin{bmatrix} \frac{-r_0*r_1+e^{-\delta}}{t_0*t_1} & \frac{-r_1*(t_0^2-r_0^2)-r_0\cdot e^{\delta}}{t_0*t_1} \\ \frac{r_1+r_0*(t_1^2-r_1^2)\cdot e^{-\delta}}{t_0*t_1} & \frac{-(r_0*r_1)+(t_0^2-r_0^2)*(t_1^2-r_1^2)\cdot e^{-\delta}}{t_0*t_1} \end{bmatrix} \quad (5.17)$$

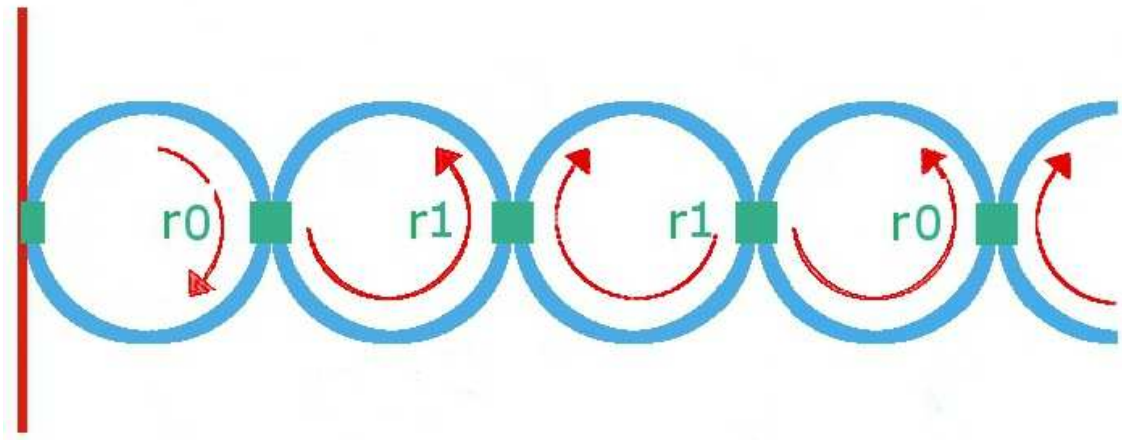

Fig 5.19 *Last group of rings of an N-Ring resonator using the second kind of symmetry.*

Now we formulate the last rings and for this we can use two matrices of the first kind of symmetry, M_{14} and M_{13}. All that is required is to multiply these two matrices to obtain the matrix formulation of the last group of rings of the second kind of symmetry.

$$M_{23} = M_{14} \cdot M_{13} = \begin{bmatrix} \left(\frac{r_1}{t_1 * t_0}\right) \cdot e^{\delta/2} - \left(\frac{r_0}{t_1 * t_0}\right) \cdot e^{-\delta/2} & \left(\frac{t_1^2 - r_1^2}{t_1 * t_0}\right) \cdot e^{\delta/2} - \left(\frac{r_0 * r_1}{t_1 * t_0}\right) \cdot e^{-\delta/2} \\ \left(\frac{r_0 * r_1}{t_1 * t_0}\right) \cdot e^{\delta/2} + \left(\frac{t_0^2 - r_0^2}{t_1 * t_0}\right) \cdot e^{-\delta/2} & \left(\frac{r_0 * (t_1^2 - r_1^2)}{t_1 * t_0}\right) \cdot e^{\delta/2} - \left(\frac{r_1 * (t_0^2 - r_0^2)}{t_1 * t_0}\right) \cdot e^{-\delta/2} \end{bmatrix} \cdot \begin{bmatrix} \frac{-r_0 * r_1 + e^{-\delta}}{t_0 * t_1} & \frac{-r_0 * (t_1^2 - r_1^2) - r_1 \cdot e^{\delta}}{t_0 * t_1} \\ \frac{r_0 + r_1 * (t_0^2 - r_0^2) \cdot e^{-\delta}}{t_0 * t_1} & \frac{-(r_0 * r_1) + (t_0^2 - r_0^2) * (t_1^2 - r_1^2) \cdot e^{-\delta}}{t_0 * t_1} \end{bmatrix} \quad (5.18)$$

Now we can easily obtain the amplitude transfer function and the relative intensity.

5.6 Second category of symmetry: Results

We examine the transfer functions for the second category of symmetry in this section and we find that the bandwidth is still very large and unworkable if we want to filter one or a few DWDM channels. If we want to design a channel dropping filter using the first symmetry category the bandwidth will be better but the depth of modulation is greater with the second category. The results are plotted in Figures 5.20 to 5.23.

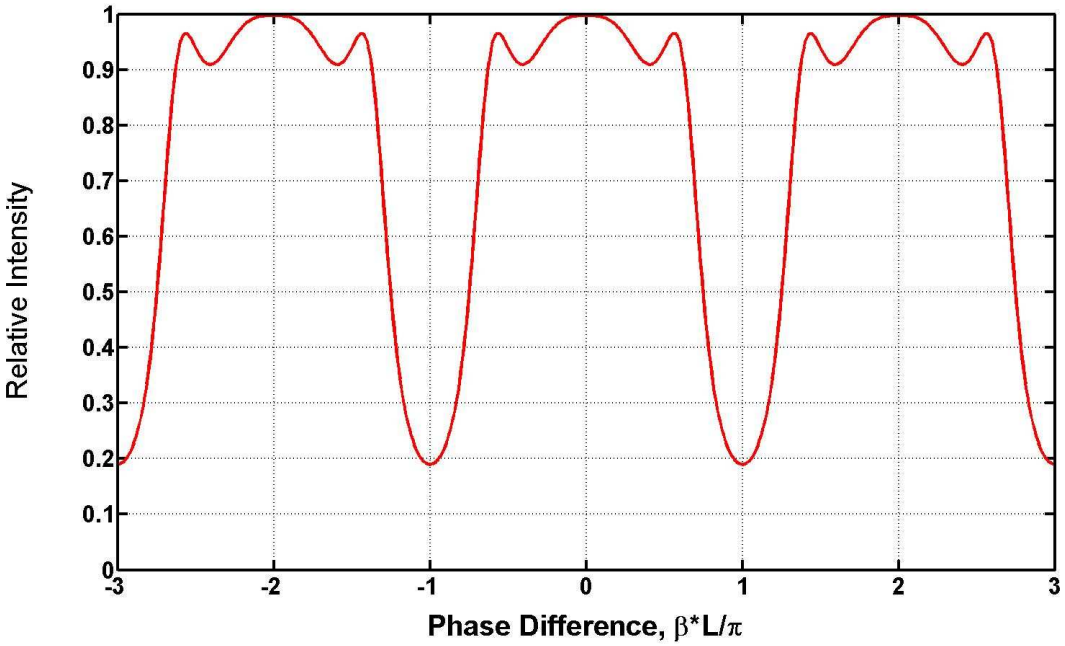

Fig 5.20 *Transfer Function in linear units for an 8-ring resonator with the second kind of symmetry with r_0 = 0.1, r_1 = 0.25 and r_2 = 0.05. The depth of modulation is 7.2 dB.*

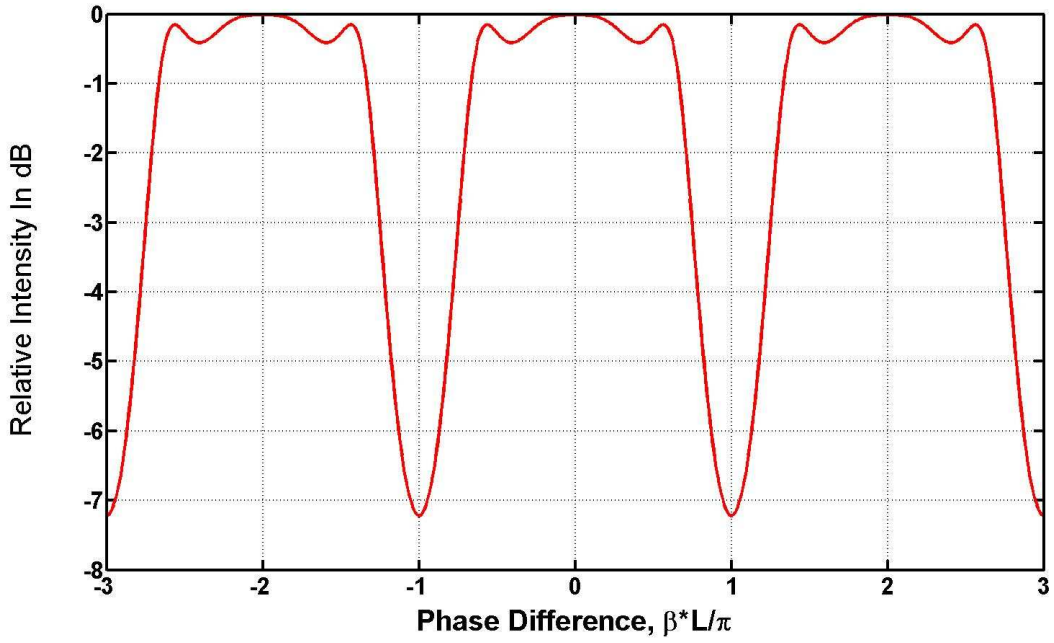

Fig 5.21 *Transfer function in dB for an 8-ring resonator with the second kind of symmetry with r_0 = 0.1, r_1 = 0.25 and r_2 = 0.05. The depth of modulation is 7.2 dB.*

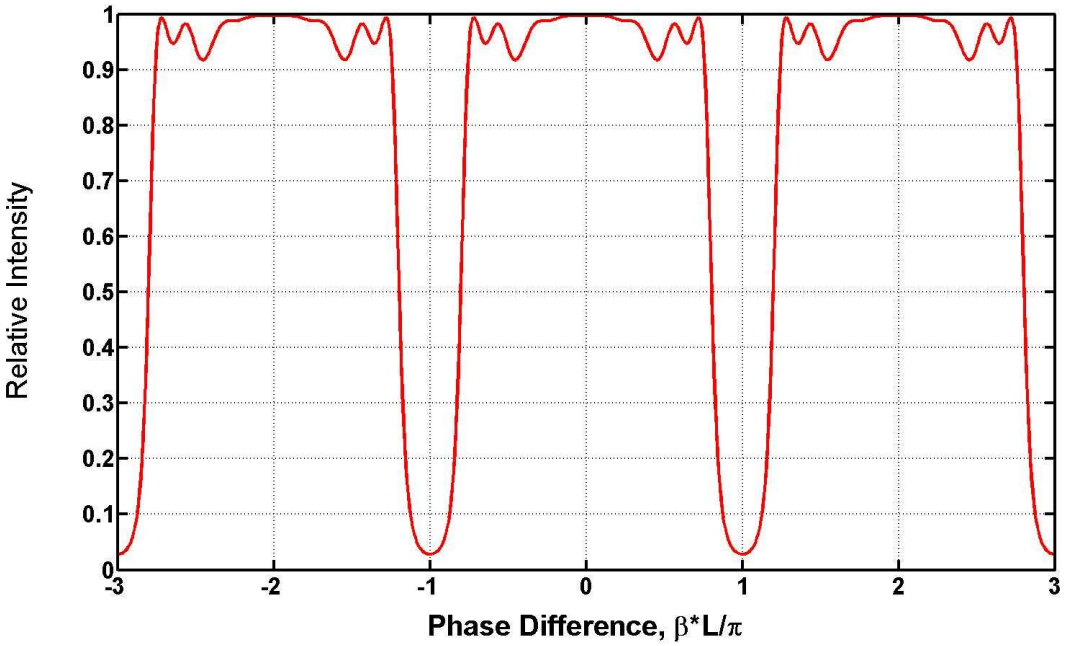

Fig 5.22 *Transfer function in linear units for a 16-Ring resonator with the second kind of symmetry with r_0 = 0.1, r_1 = 0.2 and r_2 = 0.05. The depth of modulation is 15.6 dB.*

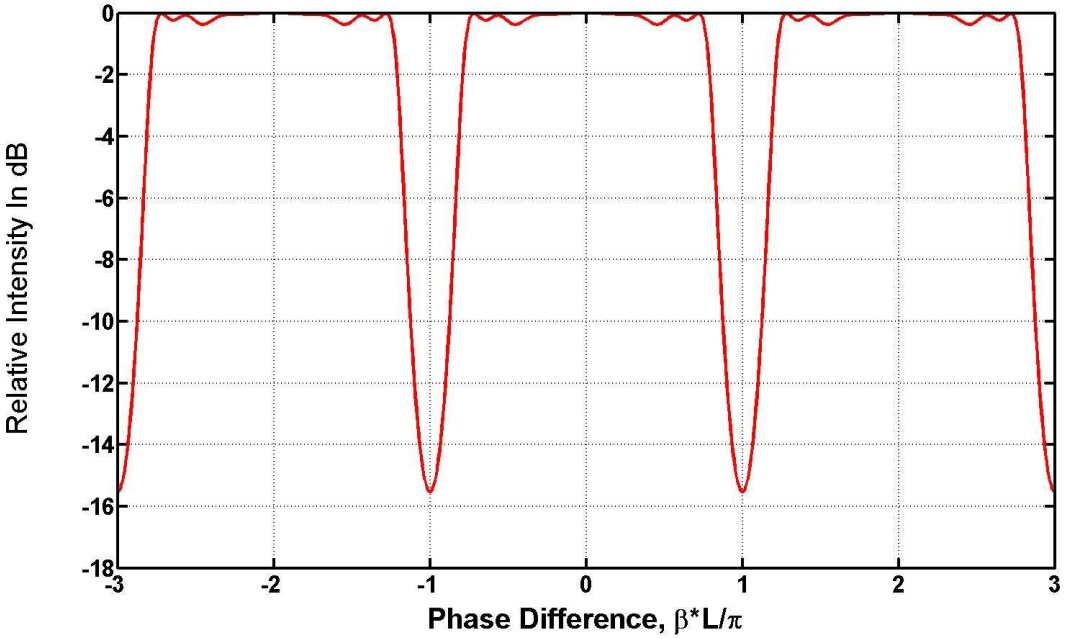

Fig 5.23 *Transfer function in dB for a 16-Ring resonator with the second kind of symmetry with r_0 = 0.1, r_1 = 0.2 and r_2 = 0.05. The depth of modulation is 15.6 dB.*

5.7 Bandwidth-passing and bandwidth-dropping characteristics

We have shown in Section 5.4 that the compound resonator makes a transition from a channel or bandwidth passing response (as shown in Figures 5.9 and 5.10) to a channel or bandwidth dropping response (as shown in Figures 5.11 and subsequently). The transition appears to occur between four and eight rings and the purpose of this section is to investigate the phenomenon. We can also observe that the bandwidth increases with the number of rings and the profile of the filter is more "box-like" with a high number of rings.

We have calculated two more transfer function with a third symmetry category. The first is a transfer function of a 6-ring resonator with $r_0 = r_2 = r_4 = r_6 = 0.2$ and $r_1 = r_3 = r_5 = 0.2$, as shown in Figure 5.24. The second is a transfer function of a 12-ring resonator with $r_0 = r_2 = r_4 = r_6 = r_8 = r_{10} = r_{12} = 0.1$ and $r_1 = r_3 = r_5 = r_7 = r_9 = r_{11} = 0.2$. These two transfer functions are also shown in Figure 5.24, together with a transfer function for an 8-ring resonator with the first symmetry category and a transfer function of a 16-ring resonator with the first symmetry category.

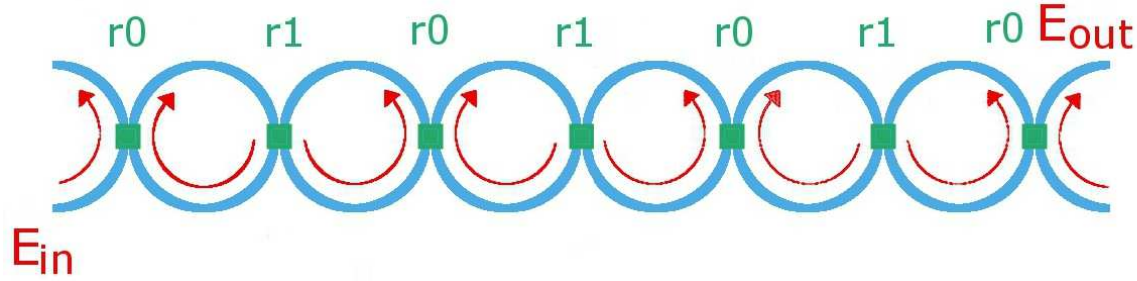

Fig 5.24 *6-Ring resonator with the third symmetry category.*

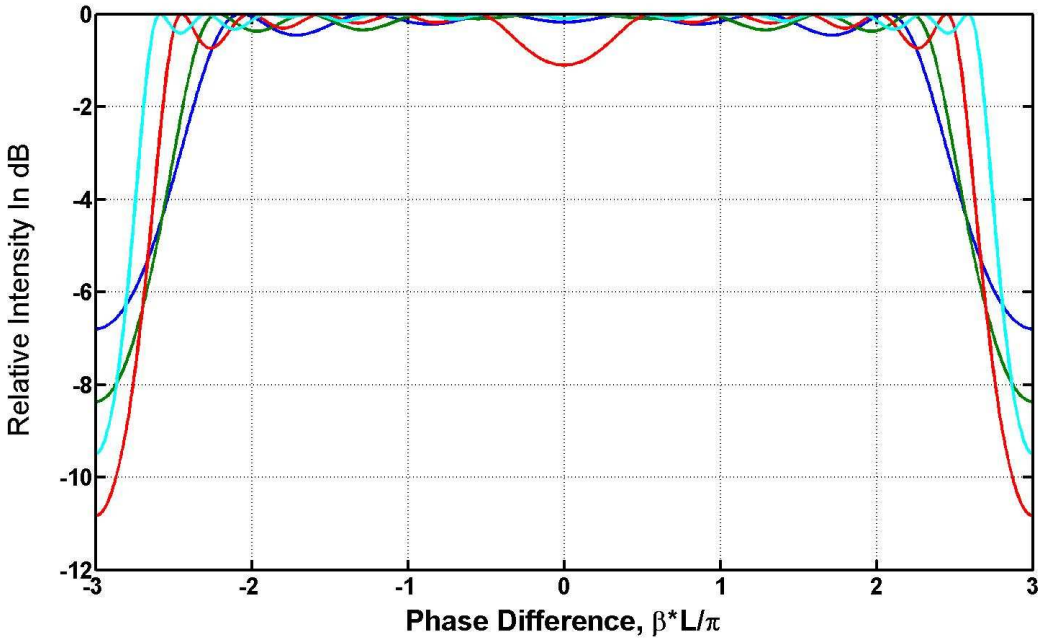

Fig 5.24 *Transfer Functions in dB for N-ring resonators*
Dark blue: N = 6, third symmetry category, r_0 = 0.2 and r_1 = 0.2.
Green: N = 8, first symmetry category, r_0 = 0.15, r_1 = 0.2 and r_2 = 0.2.
Red: N = 12, third symmetry category, r_0 = 0.1 and r_1 = 0.2.
Light Blue: N = 16, first symmetry category, r_0 = 0.1, r_1 = 0.1 and r_2 = 0.15.

In Figure 5.24 it is clear that transfer function profiles become more "box-like" when the number of rings increases. However, if we want a channel passing filter we need to find another solution. As we can notice in Equation (5.1), an alternative output exists. This output is a reflected output. If we ignore the losses we can write $|E_{out}|^2 + |E_{out\ alternative}|^2 = 1$ [5]. So we can easily move from a channel dropping filter to a channel passing filter but we have to redefine the amplitude transfer function as in Equation (5.19), the reason for which is given by Elshoff and Rautenberg [1].

$$\frac{\mathrm{E_{out\ alternative}}}{\mathrm{E_{in}}} = \frac{-\mathrm{q_{21}}}{\mathrm{q_{22}}} \qquad (5.19)$$

The relative intensity is obtained by squaring modulus of the amplitude transfer function as before.

$$\frac{I_{out\ alternative}}{I_{in}} = \left| \frac{E_{out\ alternative}}{E_{in}} \right|^2 \qquad (5.20)$$

The transfer function of the alternative output of a 16-ring resonator with the first symmetry category is shown in Figure 5.25.

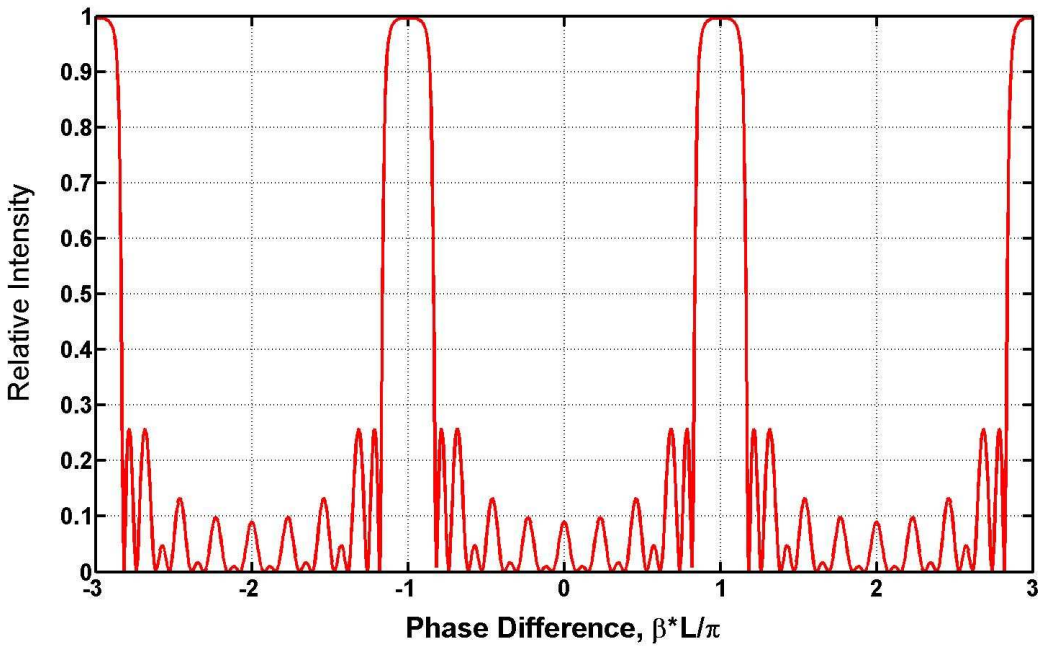

Fig 5.22 *Transfer function of the alternative output in linear units for a 16-Ring resonator with the first kind of symmetry with r_0 = 0.2, r_1 = 0.2 and r_2 = 0.3.*

In Figure 5.22 the filter profile is that of a band-pass filter and it is "box-like". Moreover the resonance peaks reach 100%, but there are many perturbations, in the form of side-bands between the peaks. Unfortunately, we did not have the time to perform more simulations to find the best coupling ratios to eliminate the perturbations. We believe that very precise coupling ratios are likely to be required. The issue of accuracy of coupling ratios is addressed further in Chapter 7.

6 Waveguide Losses And Effective Reflectance Errors

6.1 Introduction

The results that we have presented in Chapters 3 to 6 have implicitly assumed that optical rings can be fabricated with ideal couplers that have precisely defined coupling ratios and that the small radii bends necessary to create the rings do not lead to loss. In reality, neither of these assumptions is valid [8]. The purpose of this chapter is to examine, through examples, how real, but imperfect, components influence the filter performance.

6.2 Effective Reflectance Fabrication Errors

When we made our calculations we noticed that small changes to the effective reflectance can have large consequences for the transfer function. Moreover, we learned that it is very demanding to build couplers with precisely determined coupling ratios. We have therefore added a parameter precision_R to the Matlab function, as stated in Chapter 3. This parameter represents the accuracy of the coupling ratios in percentage. If, for example, we use 10 % in precision_R and we have two coupling ratios $r_0 = 0.5$ and $r_1 = 0.7$, the Matlab function computes three transfer functions. The first one with $r_0 = 0.5$ and $r_1 = 0.7$ the second with $r_0 = 0.45$ and $r_1 = 0.63$ and the last with $r_0 = 0.55$ and $r_1 = 0.77$. We begin by plotting a transfer function with two rings, as depicted on Figure 6.1. It is clear that an error of 10 % on the coupling ratio can totally change the transfer function.

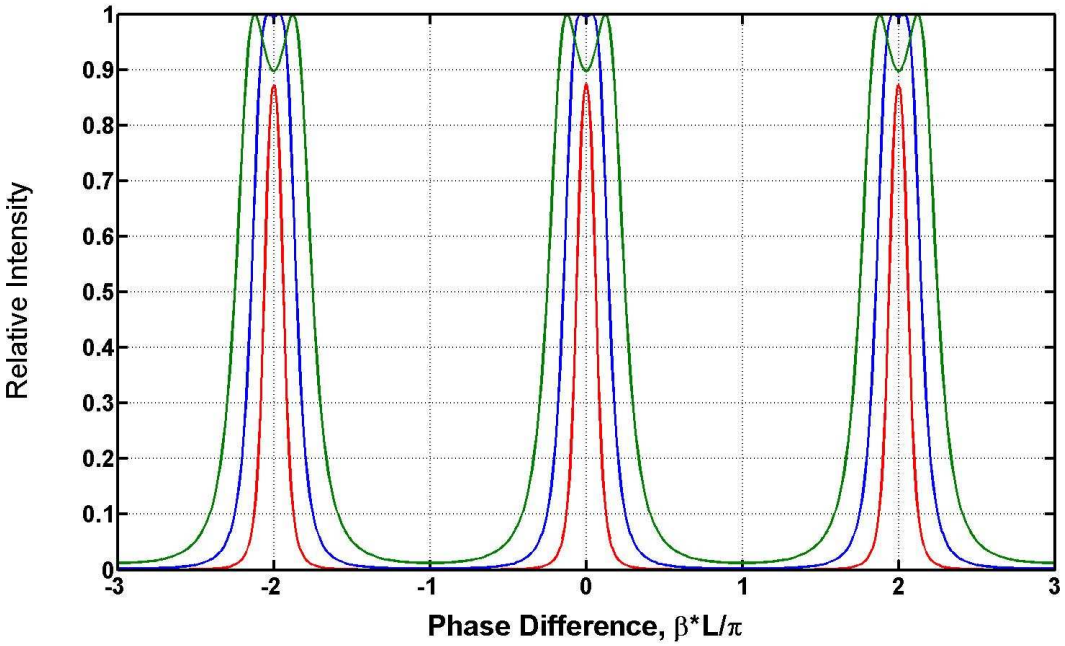

Fig 6.1 *Transfer functions in linear units: Relative intensity of a 2-ring resonator. Blue: r_0 = 0.74 and r_1 = 0.95, Green: r_0 = 0.666 and r_1 = 0.855, Red: r_0 = 814 and r1 = 0.99.*

In Figure 6.1 the blue curve represents the transfer function of a 2-ring resonator with ideal coupler but if the coupler has a coupling ratio error of 10 % either a double peak appears or the resonance peak is reduced.

We have repeated this operation with 8 and 16 rings, as shown in Figures 6.2 and 6.3.

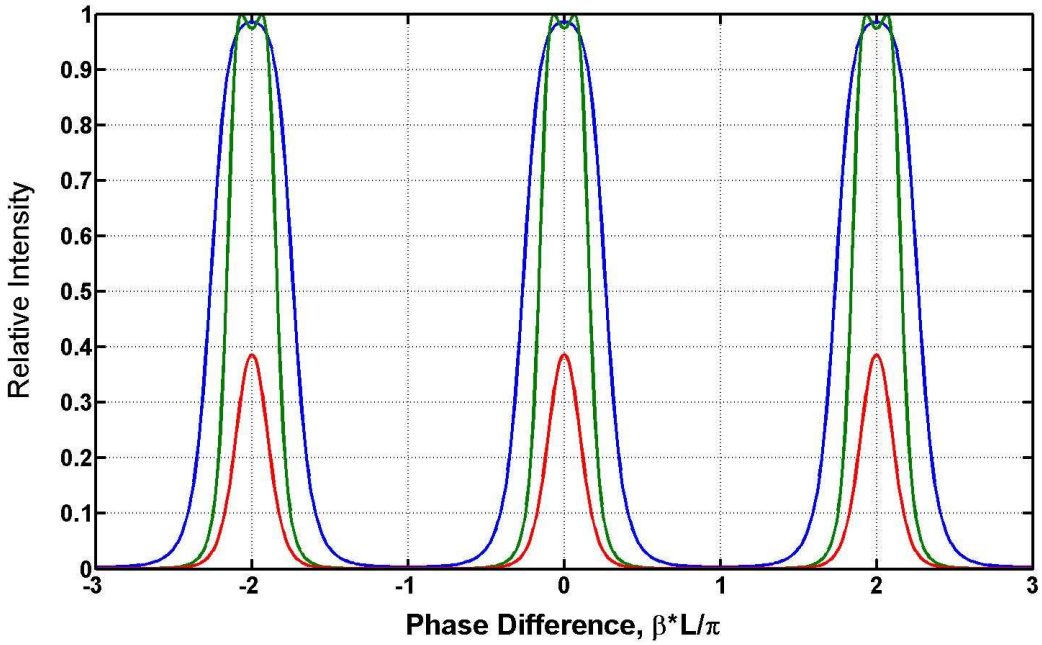

Fig 6.2 *Transfer functions in linear units: Relative intensity of a 4-ring resonator with the first symmetry category. Blue: r_0 = 0.2, r_1 = 0.65 and r2 = 0.9, Red: r_0 = 0.18, r_1 = 0.585 and r_2 = 0.81, Green: r_0 = 0.22, r_1 = 0.715 and r_2 = 0.99.*

The blue curve in Figure 6.2 represents the transfer function of a 2-ring resonator with ideal couplers but if the coupler has a coupling ratio error of 10 % either a double peak appear or the resonance peak is reduced.

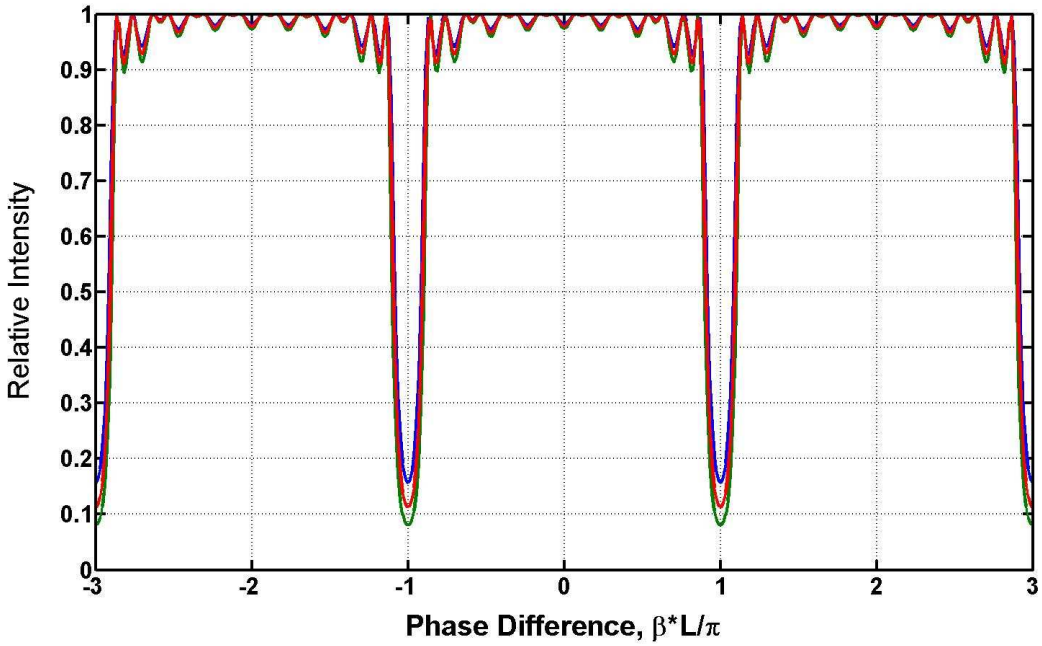

Fig 6.3 *Transfer functions in linear units: Relative intensity of a 16-ring resonator with the first symmetry category. Blue: r_0 = 0.1, r_1 = 0.1 and r_2 = 0.15, Green: r_0 = 0.09, r_1 = 0.09 and r_2 = 0.135, Red: r_0 = 0.11, r_1 = 0.11 and r_2 = 0.165.*

Figure 6.3 is the transfer function of a 16-ring resonator with coupler ratio errors. All curves are very close; the accuracy of the coupling ratios has less importance if we use a large number of rings.

Figures 6.1 to 6.2 clearly show how fabrication errors in the effective reflectance can have important consequences on the transfer function, especially with resonators that have a low number of rings. Ours plots show that the transmittance of the resonance peaks can be reduced and that there can be double peaks the degeneracy condition, to which Elshoff and Rautenberg referred, is no longer valid. Figures 6.1 to 6.3 also provide evidence that the filter characteristics are less sensitive to coupler fabrication errors when the resonator consists of a large number of rings.

6.3 Waveguide Losses

To study the influence of waveguide loss on micro-ring resonators, we consider, arbitrarily, a three-ring structure with equal circumferences. The chosen coupling ratios are K_a = 0.6 and K_b = 0.1. The study begins with a ring of circumference L equal to 200 µm. In order to obtain the most significant results, we chose a regular sequence of losses: 0, 8, 16, 24, 32, 40 dB/cm. As illustrated in Figure 6.4, the peak of the relative intensity decreases with increasing losses. Moreover, the shape of the peak changes; it become less "box like". The lower plot of Figure 6.4 is in logarithmic units, from which we can see that the minimum values at $\beta L / \pi = \pm 1$" are slightly higher when the losses are increased. This is indicative of a reduction of the depth of modulation from 38.5 dB when there is no waveguide loss to 35.1 dB at the worst loss that we consider [9].

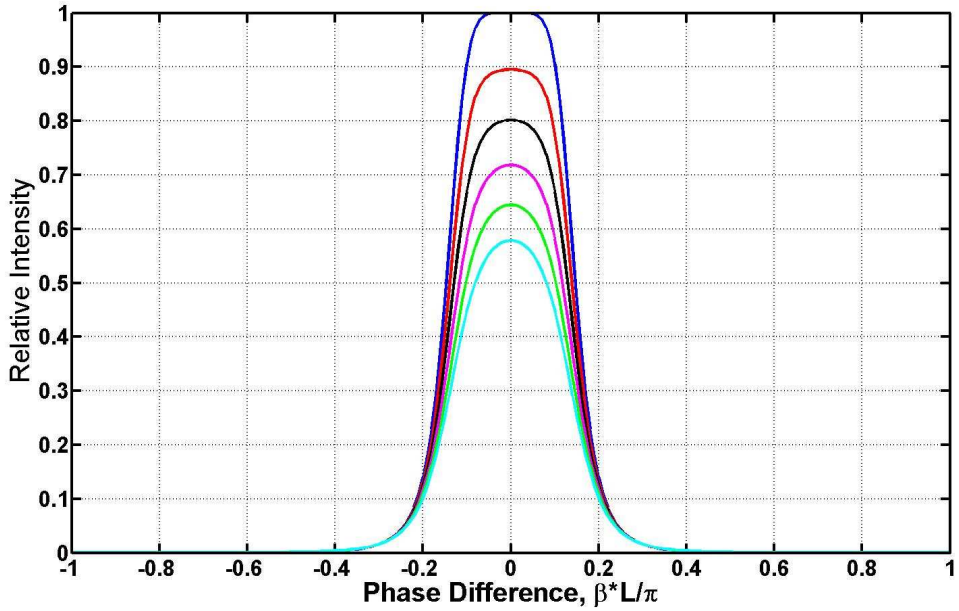

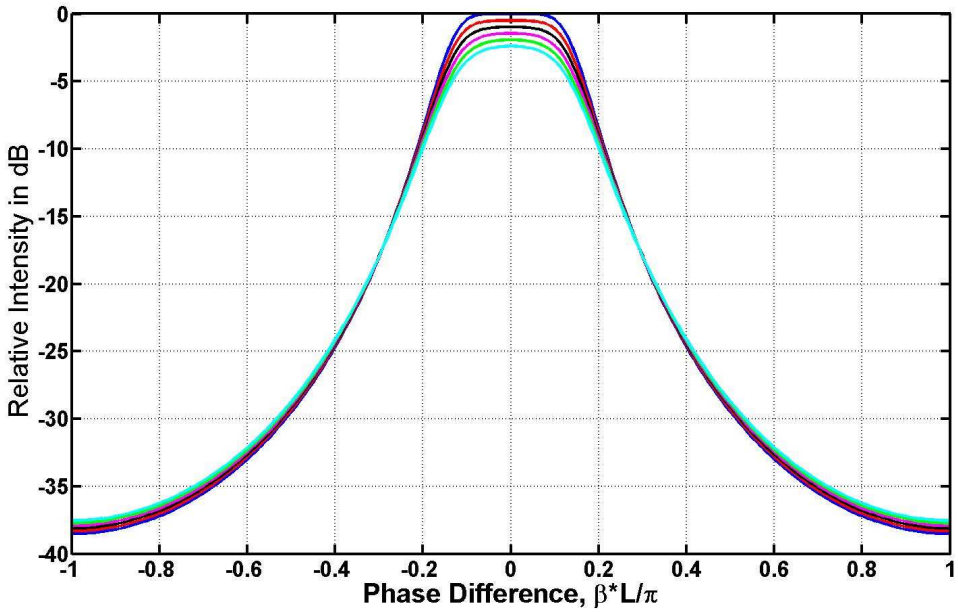

Fig 6.4 *Transfer functions of a three-ring resonator with equal ring circumferences (L= 200 µm). The coupling ratios are* K_a = 0.6 and K_b = 0.1. *The loss coefficients are (from the top to the bottom of each graph): 0, 8, 16, 24, 32 and 40 dB/cm. These curves are plotted on linear and decibel vertical axes.*

We take the peak heights and plot them on a graph in order to obtain the curve "Peak heights" versus "waveguide loss". The result is plotted in Figure 6.5, from which it appears that the peak height is not proportional to the waveguide loss; there is a slight curvature.

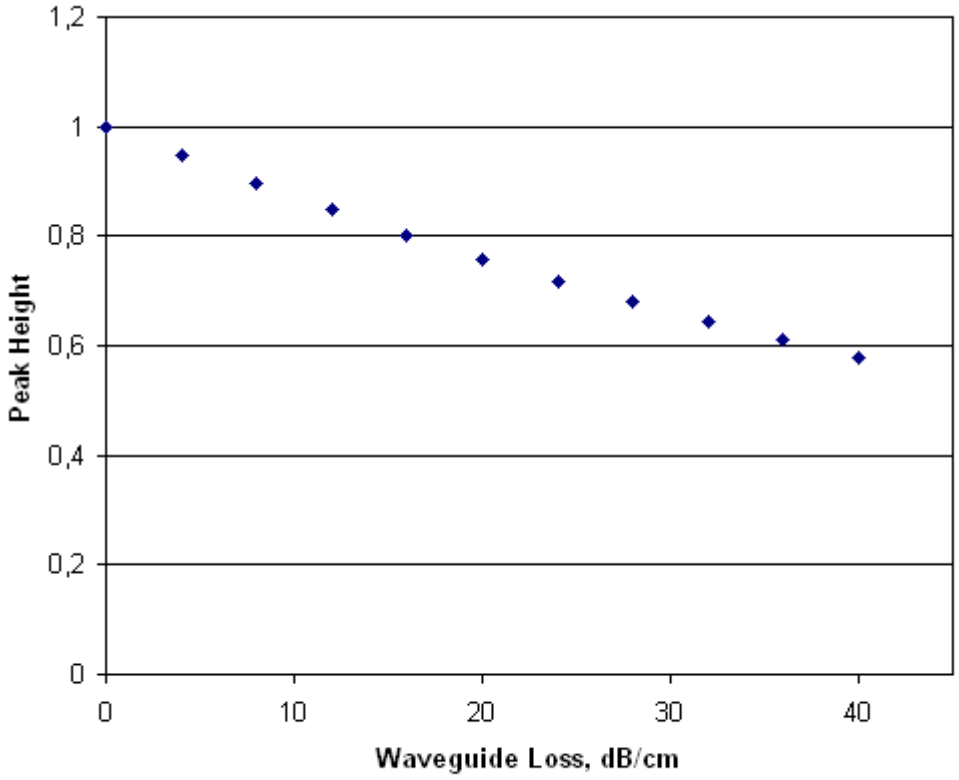

Fig 6.5 Representation of the transfer function peak height versus the waveguide loss.

In this section, we have shown that waveguide loss deteriorates the performance of compound micro-ring resonators. Their resonance peaks, depth of modulation and box-like profiles are all diminished. However, we have examined a very wide range of loss coefficients and we are therefore optimistic that it will be possible to achieve very useful filtering performance with appropriate fabrication techniques and waveguide materials and design.

7 Application Of A Bipolar Non Return To Zero Code

7.1 Optical Modulation Formats

The majority of optical fibre communication is in the form of digital transmission, where the data is encoded into discrete states of power, phase or polarization. There are now many modulation formats, which range from simple on/off keying to sophisticated methods that impose phase and polarization changes. They are formats that use multiple power levels for the signal or suppress one side-band. Some formats perform better in the presence of high chromatic dispersion, non linear optical effects or amplifier noise, while others have lower modulated bandwidths and therefore permit greater channel densities. The subject of optical modulation formats is therefore currently an active area of research [10],[11].

We believe that one of the main justifications for ring resonators is that they permit the design of a range of different pass-band profiles, which could be used in conjunction with the newer optical modulation formats for digital data. In this Chapter we study one application out of many possibilities for future research. We consider a bipolar non-return-to-zero code, the modulation bandwidths of the channels when it is used and how a ring resonator can be used to select a subset of these channels.

7.2 Bipolar Non Return To Zero Code

The bipolar non return to zero code also, called bipolar NRZ code, is one of the modulation formats being explored for DWDM. It is why we chose this code to show an application of the ring resonator.

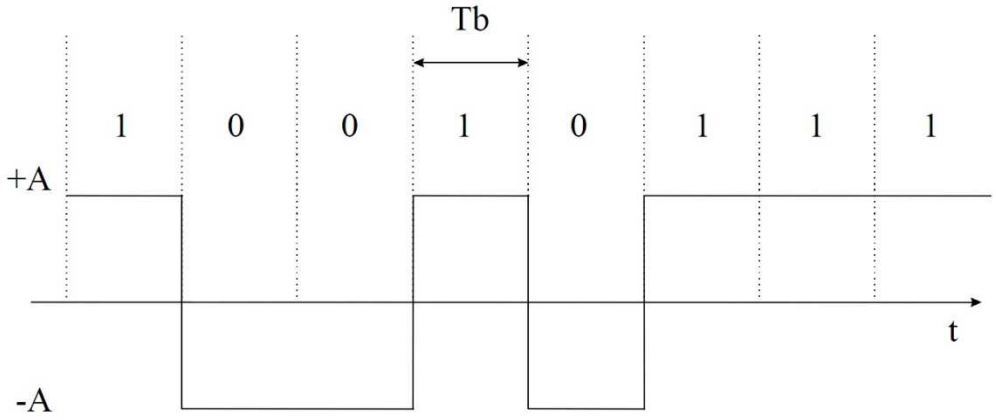

Fig 7.1 *NRZ bipolar code using a rectangular pulse and period* T_b. *It associates the bit '0' to the amplitude -A and the bit '1' to the amplitude +A* [12].

To have a good view of the bipolar NRZ code we need to plot the spectral density, as illustrated in Figure 7.2.

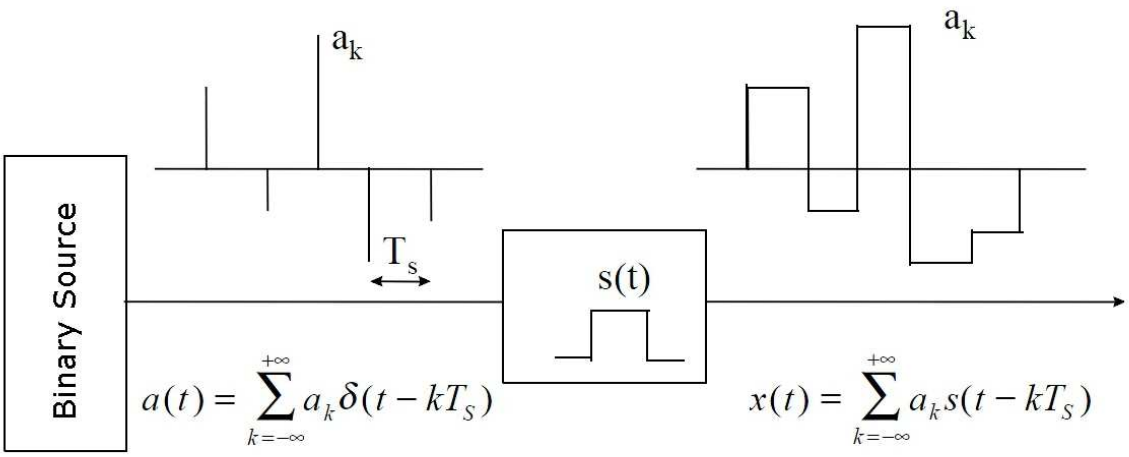

Fig 7.2 *Representation of the binary random sequence a_k and the coded signal x(t)* [12].

We called $R_a(m)$ the autocorrelation function of the random sequence a_k and $S_a(f)$ the Fourier transform of R_a which is show Equation (7.1) [12].

$$R_a(m) = E(a_k a_{k-m}^*) \tag{7.1}$$

The elementary pulse s(t) is written as Equation (7.2).

$$s(t) = \text{rect}_{Tb}\left(t - \frac{Tb}{2}\right) \tag{7.2}$$

The notation $rect_T(t)$ represents a rectangular function with an amplitude of 1 and a period T, such as $rect_T(t) = 1$ if $-\frac{T}{2} \leq t \leq \frac{T}{2}$ and $rect_T(t) = 0$ otherwise.

To find the spectral density we can use the Bennett formula which is stated as equation (7.3).

$$S_x(f) = \frac{1}{T_s}|S(f)|^2 \sum_{m=-\infty}^{+\infty} R_a(m)\, e^{-2\pi j f m T_s} \qquad (7.3)$$

Where,

$$S_x(f) = \frac{1}{T_s}|S(f)|^2 S_a(f) \qquad (7.4)$$

and

$$R_a(0) = \sigma_a^2 + m_a^2 \qquad (7.5)$$

$$R_a(k) = E(a_n a_{n-k}^*) = m_a^2 \text{ if } k \neq 0 \qquad (7.6)$$

$$S_a(f) = \sum_{k=-\infty}^{+\infty} R_a(m)\, e^{-2\pi j f k T_s} \qquad (7.7)$$

$$S_a(f) = \sigma_a^2 + m_a^2 \sum_{k=-\infty}^{+\infty} e^{-2\pi j f k T_s} \qquad (7.8)$$

$$S_a(f) = \sigma_a^2 + \frac{m_a^2}{T_s^2} \sum_{k=-\infty}^{+\infty} \delta\left(f - \frac{k}{T_s}\right) \qquad (7.9)$$

If the symbols a_k are independent, we can easily write m_a as in Equation (7.10).

$$m_a = E(a_k) = A * p(1) - A * p(0)$$
$$= A * (p(1) - p(0)) \qquad (7.10)$$

with A the amplitude of the NRZ signal, p(1) the probability to obtain a '1' and p(0) the probability to obtain a '0'.

On average, there as many "ones" as "zeros" and so we can consider that p(1) = p(0) = 0.5. Then,

$$m_a = 0 \tag{7.11}$$

$$R_a(0) = E\left(a_k^2\right) = A^2 \tag{7.12}$$

$$\sigma_a^2 = R_a(0) - m_a^2 \text{ , } \sigma_a^2 = R_a(0) = A^2 \tag{7.13}$$

If we substitute Equations (7.11) and (7.13) into Equation (7.9) we have:

$$S_a(f) = A^2 \tag{7.14}$$

The Fourier transform of the elementary pulse (Equation (7.2)) is given by Equation (7.15).

$$S(f) = T_b \frac{\sin(\pi f T_b)}{\pi f T_b} e^{-j\pi f T_b} \tag{7.15}$$

If we substitute Equations (7.16) and (7.14) into Equation (7.4) we obtain the power spectral density of a NRZ signal as given by Equation (7.17).

$$S_{NRZ}(f) = \frac{1}{T_b}\left|T_b \frac{\sin(\pi f T_b)}{\pi f T_b} e^{-j\pi f T_b}\right|^2 \cdot A^2 \tag{7.17}$$

$$S_{NRZ}(f) = T_b \left(\frac{\sin(\pi f T_b)}{\pi f T_b}\right)^2 \cdot A^2 \tag{7.18}$$

Figure 7.3 is a plot of twenty one channels from a DWDM system in which channel spacing is 50 GHz in accordance with the ITU-T Standard [3].

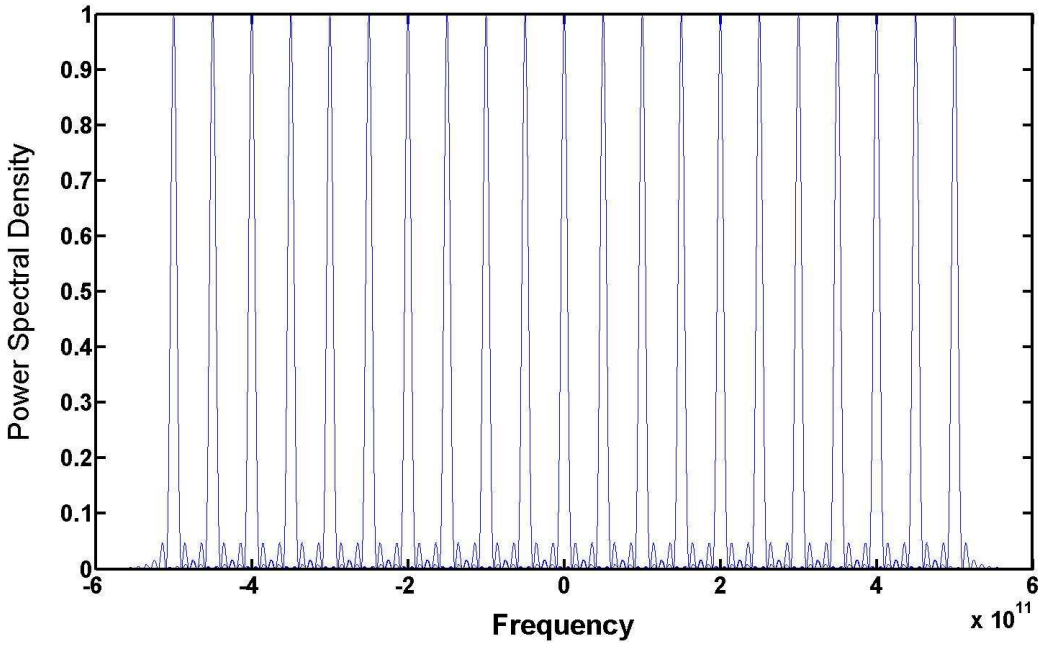

Fig 7.3 *Power Spectral Density of 21bipolar NRZ signals with a channel spacing of 50 GHz as a function of the frequency.*

7.3 Ring Resonator application

We have designed a simple filter which can be applied to bipolar NRZ signals. We concentrate our research on four-ring resonators because Elshoff and Rautenberg have already studied one, two and three ring structures with rings that have the same circumference.

The filter that we designed is with an FSR of 100 GHz, so we choose to filter one channel out of two as we can see on Figure 7.4. Thanks to Equation (2.7) we can easily find the circumference we need to assure the FSR of 100GHz:

$$L = \frac{c}{n_{eff} * FSR} = \frac{3*10^8}{1.5*10^{11}} = 5 * 10^{-4} \text{ meters} = 500 \text{ µm} \quad (7.22)$$

The circumference that we used is 500 µm and we ignored the losses of the waveguides and couplers.

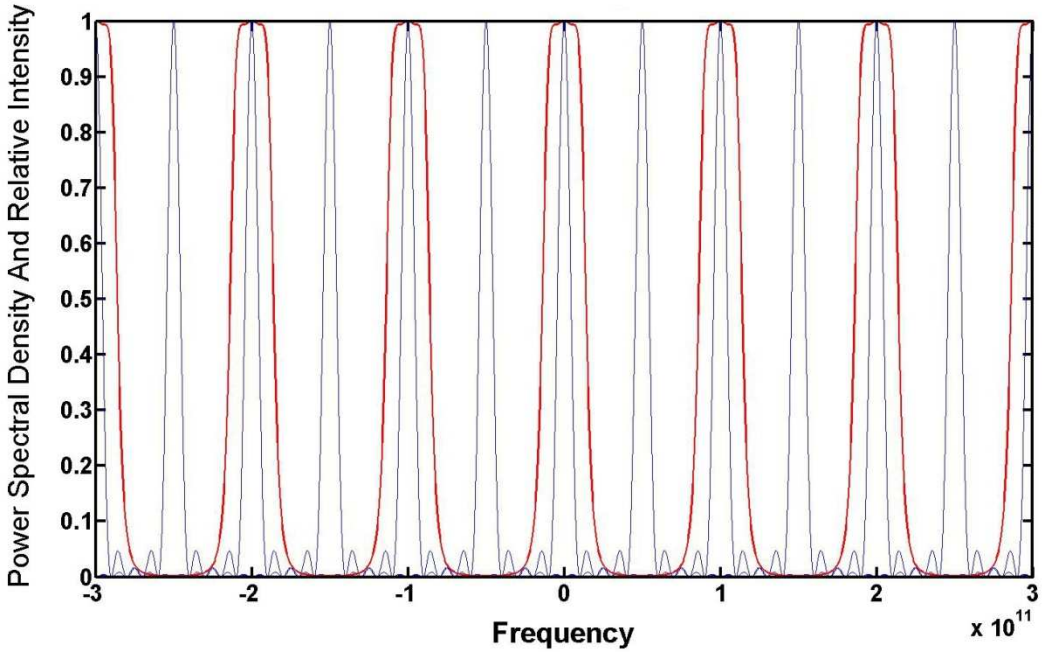

Fig 6.3 Blue: *Power spectral density of 12 bipolar NRZ signals with a channel separation of 50 GHz.*
Red: The transfer function of a 4-ring resonator with an FSR of 100 GHz. The effective reflectances are $r_0 = 0.1$, $r_1 = 0.56$, $r_2 = 0.84$, $r_3 = 0.86$ *and* $r_4 = 0.55$.

Figure 6.3 shows how a periodic filter with box-like pass bands can be constructed from compound ring resonators to accept a pre-determined sub-set of transmitted DWDM channels. It illustrates why the single ring resonator transfer profiles described in Chapter 2 are not suitable for this application. Multiple compound rings provide us with the design flexibility to select the desired channels with a minimum of spectral distortion but, through the provision of high depths of modulation, to reject the unwanted channels.

8 Conclusion

This Project is a theoretical study of compound micro-optical ring resonators for application as channel selecting filters in DWDM optical communications. We have compared a number of design possibilities. We have simulated all of the filters that we studied numerically and compared our results with an analytical model. That way, we were more confident about the veracity of the transfer functions calculated.

We have investigated the benefits that the Vernier effect could provide for the design of three- and four-ring resonators. This particular effect can increase the performances of these two kinds of resonators in many ways: more "box like" filters, greater depth of modulations and more adaptive filters. Especially in the three-ring resonator configuration, the Vernier effect provides filters with high sideband suppression ratios. The disadvantage is that the couplers used are of extreme values, therefore, they could have low production yields.

We have calculated, using the matrix technique, the transfer functions of N-ring resonators with two different kinds of symmetries. With an increasing number of rings, we obtain a more "box like" filter shape. We also obtain an increasing filter bandwidth, which is an issue, because thus, it is more difficult to select only one channel. The solution we gave is to use the alternative output (also called auxiliary output) of the micro-rings. Unfortunately, this solution provided some unwanted side-bands in the transfer functions, and we did not have enough time to find a way to eliminate them.

We have also studied the influence of losses and the fabrication accuracy of the effective reflectance on micro-ring resonators. They could reduce the performance of the transfer function. Effective reflectances that deviate from the design target diminish the peak of resonance or create two sub-peaks as well. We have found that the effect is most marked in resonators that have a small number of rings. We have also shown that waveguide loss reduces the transmission peaks of the transfer function and renders them less “box like”. Consequently, the study of their influence was of great importance for future experimental demonstrations of our results.

We have presented an example showing that micro-ring resonators can filter DWDM channels to a very high standard. We modeled the means to reject one of two DWDM channels coded by a bipolar Non Return to Zero code (bipolar NRZ code). This was a more concrete task, which was very satisfying after all the theoretical work we realised.

In conclusion, we have obtained encouraging and original results with our designs and explorations of several kinds of micro-ring resonators. We think that the study we realised deserve to be pursued because further improvement can be made with further use of optimisation.

Appendix 1: Formulation Of A Four-Ring Resonator

In this appendix we state the general transfer function for a four-ring resonator by Paul Urquhart. The method used is an extension of the matrix approach described by Elshoff and Rautenberg.

To do that Urquhart used the matrix technique to formulate the electric field transfer function. Thereafter, he multiplied the field transfer function by its own complex conjugate to obtain the intensity transfer function. It is important to say that he did not make assumptions about equality of the ring circumferences or negligible loss. The intensity equation is very long and it is listed here in Matlab-compatible format.

```
t0= i*sqrt(1-r0^2);
t1= i*sqrt(1-r1^2);
t2= i*sqrt(1-r2^2);
t3= i*sqrt(1-r3^2);
t4= i*sqrt(1-r4^2);

R01=r0*r1;
R12=r1*r2;
R23=r2*r3;
R34=r3*r4;
R02=r0*(t1^2-r1^2)*r2;
R13=r1*(t2^2-r2^2)*r3;
R24=r2*(t3^2-r3^2)*r4;
R03=r0*(t1^2-r1^2)*(t2^2-r2^2)*r3;
R14=r1*(t2^2-r2^2)*(t3^2-r3^2)*r4;
R04=r0*(t1^2-r1^2)*(t2^2-r2^2)*(t3^2-r3^2)*r4;
```

The numerator N :

```
N=abs(t0^2*t1^2*t2^2*t3^2*t4^2);
```

R=(1-R01-R12-R23-R34-R02-R13-R24-R03-R14-
R04+R01*R34+R01*R23+R12*R34+R01*R24+R02*R34)^2;

The Denominator D:
D=R
+ 4*(R01*(1+R23^2+R24^2+R34^2)-R12*R02*(1+R34^2)-
(R13*R03+R14*R04)).*sin(teta1./2).^2+ 4*((R12-R01*R02)*(1+R34^2)
+R01*(R23*R03+R24*R04)-(R13*R23+R14*R24)).*sin(teta2./2).^2+
4*((R23-R24*R34)*(1+R01^2)+R34*(R02*R04+R12*R14)-
(R02*R03+R12*R13)).*sin(teta3./2).^2+4*(R34*(1+R01^2+R12^2+R02
^2)-R23*R24*(1+R01^2)-(R03*R04+R13*R14)).*sin(teta4./2).^2 +
4*(R02*(1+R34^2)-(R03*R23+R04*R24)).*sin((teta1+teta2)./2).^2 +
4*(R01*(R24*R34-R23)+R12*(R04*R34-R03)).*sin((teta1+teta3)./2).^2
+ 4*(R01*R23*R24+R12*R02*R34-R01*R34-
R13*R04).*sin((teta1+teta4)./2).^2 + 4*(R04*R01*R34+R13-R03*R01-
R14*R34).*sin((teta2+teta3)./2).^2 + 4*((R02*R01-
R12)*R34+(R04*R01-R14)*R23).*sin((teta2+teta4)./2).^2 +
4*(R24*(1+R01^2)-(R12*R14+R02*R04)).*sin((teta3+teta4)./2).^2 +
4*(R01*(R13*R23+R14*R24)-R01*R12*(1+R34^2)).*sin((teta1-
teta2)./2).^2 + 4*(R01*(R24*R34-R23)+R02*(R14*R34-
R13)).*sin((teta1-teta3)./2).^2 + 4*(R23*R24*R01+R02*R12*R34-
R01*R34-R03*R14).*sin((teta1-teta4)./2).^2 + 4*(R23-
R24*R34)*(R01*R02-R12).*sin((teta2-teta3)./2).^2 +
4*(R03*R24*R01+R02*R01*R34-R12*R34-R13*R24).*sin((teta2-
teta4)./2).^2 + 4*R34*((R02*R03+R12*R13)-
R23*(1+R01^2)).*sin((teta3-teta4)./2).^2 + 4*(R03-
R34*R04).*sin((teta1+teta2+teta3)./2).^2 -
4*(R02*R34+R23*R04).*sin((teta1+teta2+teta4)./2).^2 -
4*(R01*R24+R12*R04).*sin((teta1+teta3+teta4)./2).^2 + 4*(R14-
R01*R04).*sin((teta2+teta3+teta4)./2).^2 + 4*R01*(R14*R34-
R13).*sin((-teta1+teta2+teta3)./2).^2 + 4*R01*R12*(R23-
R24*R34).*sin((teta1-teta2+teta3)./2).^2 + 4*(R02*R24*R34-
R02*R23).*sin((teta1+teta2-teta3)./2).^2 +
4*R01*(R12*R34+R23*R14).*sin((-teta1+teta2+teta4)./2).^2 +
4*R01*(R12*R34+R13*R24).*sin((teta1-teta2+teta4)./2).^2 -
4*(R02*R34+R24*R03).*sin((teta1+teta2-teta4)./2).^2 -
4*(R24*R01+R14*R02).*sin((-teta1+teta3+teta4)./2).^2 +
4*R34*(R23*R01+R02*R13).*sin((teta1-teta3+teta4)./2).^2 +
4*R34*(R23*R01+R03*R12).*sin((teta1+teta3-teta4)./2).^2 +

```
4*R24*(R02*R01-R12).*sin((-teta2+teta3+teta4)./2).^2 +
4*R23*R34*(R12-R01*R02).*sin((teta2-teta3+teta4)./2).^2 +
4*R34*(R03*R01-R13).*sin((teta2+teta3-teta4)./2).^2 +
4*R04.*sin((teta1+teta2+teta3+teta4)./2).^2 - 4*R14*R01.*sin((-
teta1+teta2+teta3+teta4)./2).^2 + 4*R01*R12*R24.*sin((teta1-
teta2+teta3+teta4)./2).^2 + 4*R23*R02*R34.*sin((teta1+teta2-
teta3+teta4)./2).^2 - 4*R03*R34.*sin((teta1+teta2+teta3-
teta4)./2).^2 - 4*R02*R24.*sin((-teta1-teta2+teta3+teta4)./2).^2 -
4*R01*R12*R23*R34.*sin((-teta1+teta2-teta3+teta4)./2).^2 +
4*R01*R13*R34.*sin((-teta1+teta2+teta3-teta4)./2).^2;
```

$$\frac{I_{out}}{I_{in}} = \frac{N}{D}$$

List of references

[1] M. Elshoff, O. Rautenberg, "Design And Modelling Of Ring Resonator Used As Optical Filters For Communications Applications ", Project Report, Universidad Pública de Navarra, Pamplona, Spain, (2010).
[2] ITU-T Recommendation G694.2, "Spectral Grid for WDM Applications: CWDM Frequency Grid".
[3] ITU-T Recommendation G694.1, "Spectral Grid for WDM Applications: DWDM Frequency Grid".
[4] ITU-T Recommendation B15, "Nomenclature Of The Frequency And The Wavelength Bands Used In Telecommunication".
[5] P. Urquhart, "Passive Components For Optical Communications", Lecture slides, Universidad Pública de Navarra, Spain, (2009).
[6] B. Mellish, "Vernier Scale", Figure 4.1, Wikipédia.
[7] D. G. Rabus, "Integrated Ring Resonators: The Compendium".
[8] J. Park, T. Lee, D. Lee, S. Kim, W. Hwang, and Y. Chung, "Widely Tunable Coupled-Ring-Reflector Filter Based on Planar Polymer Waveguide", IEEE Photonics Technology Letters, Vol. 20, No. 12, June 15, 2008.
[9] P. Urquhart, "Introduction To Optical Telecommunications: Optical Fibre Waveguide", Lecture slides, Universidad Pública de Navarra, Spain, (2009).
[10] I. P. Kaminow and T. Li, "Optical Fiber Telecommunication, IV B: Systems And Impairment", 2002.
[11] I. P. Kaminow, T. Li and A. E. Willner, "Optical Fiber Telecommunication, B: Systems And Network", 2008.
[12] G. Baudoin, "Communications Numérique", Lecture handout, ESIEE Paris, Noisy Le Grand, France, (2006).